

Quantifying the RNA cap epitranscriptome reveals novel caps in cellular and viral RNA

Wang, Jin; Chew, Alvin Bing Liang; Lai, Yong; Dong, Hongping; Xu, Luang; Balamkundu, Seetharamsingh; Cai, Maggie Weiling; Cui, Liang; Liu, Chuan Fa; Fu, Xin-Yuan; Lin, Zhenguo; Shi, Pei-Yong; Lu, Timothy K.; Luo, Dahai; Jaffrey, Samie R.; Dedon, Peter C.

2019

Wang, J., Chew, A. B. L., Lai, Y., Dong, H., Xu, L., Balamkundu, S., . . . Dedon, P. C. (2019). Quantifying the RNA cap epitranscriptome reveals novel caps in cellular and viral RNA. *Nucleic Acids Research*, 47(20), e130-. doi:10.1093/nar/gkz751

<https://hdl.handle.net/10356/142174>

<https://doi.org/10.1093/nar/gkz751>

© 2019 The Author(s) (Published by Oxford University Press on behalf of Nucleic Acids Research). This is an Open Access article distributed under the terms of the Creative Commons Attribution Non-Commercial License (<http://creativecommons.org/licenses/by-nc/4.0/>), which permits non-commercial re-use, distribution, and reproduction in any medium, provided the original work is properly cited. For commercial re-use, please contact journals.permissions@oup.com

Downloaded on 27 Aug 2022 22:20:03 SGT

Quantifying the RNA cap epitranscriptome reveals novel caps in cellular and viral RNA

Jin Wang^{1,2,3,*}, Bing Liang Alvin Chew^{3,4,5}, Yong Lai³, Hongping Dong⁶, Luang Xu⁷, Seetharamsingh Balamkundu^{3,8}, Weiling Maggie Cai^{3,9}, Liang Cui³, Chuan Fa Liu⁸, Xin-Yuan Fu⁷, Zhenguo Lin¹⁰, Pei-Yong Shi¹¹, Timothy K. Lu^{12,13}, Dahai Luo¹⁴, Samie R. Jaffrey¹³ and Peter C. Dedon^{3,14,*}

¹State Key Laboratory of Reproductive Regulation and Breeding of Grassland Livestock, Inner Mongolia University, Hohhot, People's Republic of China, ²School of Life Sciences, Inner Mongolia University, Hohhot, People's Republic of China, ³Antimicrobial Resistance Interdisciplinary Research Group, Singapore-MIT Alliance for Research and Technology, Singapore, ⁴Lee Kong Chian School of Medicine, Nanyang Technological University, Singapore, ⁵NTU Institute of Health Technologies, Interdisciplinary Graduate Programme, Nanyang Technological University, Singapore, ⁶Shanghai Blueray Biopharma, Shanghai, People's Republic of China, ⁷Cancer Science Institute of Singapore, Singapore, ⁸School of Biological Sciences, Nanyang Technological University, Singapore, ⁹Department of Microbiology, National University of Singapore, Singapore, ¹⁰Department of Biology, Saint Louis University, St. Louis, MO, USA, ¹¹Departments of Biochemistry & Molecular Biology and Pharmacology & Toxicology, and Sealy Center for Structural Biology & Molecular Biophysics, University of Texas Medical Branch, Galveston, TX, USA, ¹²Synthetic Biology Center, Departments of Biological Engineering and Electrical Engineering and Computer Science, Massachusetts Institute of Technology, Cambridge, MA, USA, ¹³Department of Pharmacology, Weill Medical College, Cornell University, New York, NY, USA and ¹⁴Dept. of Biological Engineering, Massachusetts Institute of Technology, Cambridge, MA, USA

Received April 07, 2019; Revised July 16, 2019; Editorial Decision August 18, 2019; Accepted August 23, 2019

ABSTRACT

Chemical modification of transcripts with 5' caps occurs in all organisms. Here, we report a systems-level mass spectrometry-based technique, CapQuant, for quantitative analysis of an organism's cap epitranscriptome. The method was piloted with 21 canonical caps—m⁷GpppN, m⁷GpppNm, GpppN, GpppNm, and m^{2,2',7}GpppG—and 5 'metabolite' caps—NAD, FAD, UDP-Glc, UDP-GlcNAc, and dpCoA. Applying CapQuant to RNA from purified dengue virus, *Escherichia coli*, yeast, mouse tissues, and human cells, we discovered new cap structures in humans and mice (FAD, UDP-Glc, UDP-GlcNAc, and m⁷Gpppm⁶A), cell- and tissue-specific variations in cap methylation, and high proportions of caps lacking 2'-O-methylation (m⁷Gpppm⁶A in mammals, m⁷GpppA in dengue virus). While substantial Dimroth-induced loss of m¹A and m¹Am arose with specific RNA processing conditions, human lymphoblast cells showed no detectable m¹A or m¹Am in caps. CapQuant accurately captured the prefer-

ence for purine nucleotides at eukaryotic transcription start sites and the correlation between metabolite levels and metabolite caps.

INTRODUCTION

Nearly all forms of RNA are post-transcriptionally modified on the nucleobases or ribose (1), including the 5'-terminal 'caps' on messenger (mRNA) and other RNAs (2). The canonical cap on most eukaryotic and viral mRNAs is comprised of N⁷-methylguanosine (m⁷G) linked to the first nucleotide of the RNA by a reverse 5'-5' triphosphate bridge (Figure 1A) (2). This m⁷GpppX cap in its various forms (2) is absent in bacterial and archaeal transcripts. In many lower eukaryotes, including yeast, mRNAs contain mainly m⁷GpppN (cap 0), whereas in higher eukaryotes, the 5' penultimate and antepenultimate nucleotides can be 2'-O-methylated to different extents to generate m⁷GpppNm (cap 1) and m⁷GpppNmpNm (cap 2) structures (2). The m⁷GpppX cap has several important biological functions, such as protecting mRNA from degradation by 5'-exoribonucleases, directing pre-mRNA splicing and nuclear mRNA export, facilitating recognition by eukaryotic translation initiation factor 4E, and regulating various

*To whom correspondence should be addressed. Tel: +1 617 253 8017; Fax: +1 617 324 5280; Email: pcdedon@mit.edu
Correspondence may also be addressed to Jin Wang. Tel: +86 471 499 2435; Fax: +86 471 499 2278; Email: jinwang@imu.edu.cn

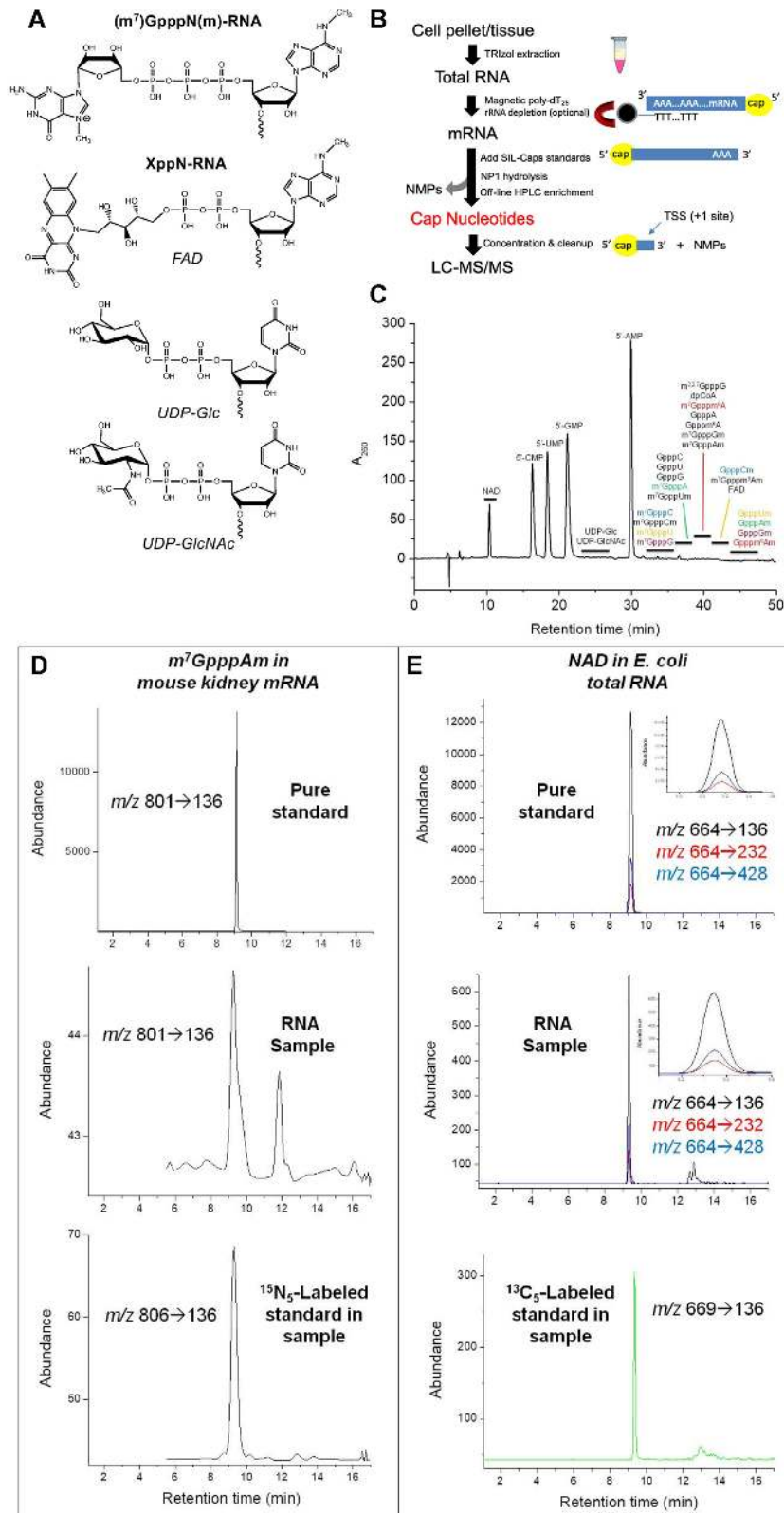


Figure 1. Analysis of 5' cap structures in RNA by CapQuant. (A) Chemical structures of 5' caps. (B) Workflow for CapQuant applied to eukaryotic mRNA. (C) A representative HPLC trace for the separation of the enzymatic digestion mixture of RNA. (D, E) Illustration of CapQuant for m^7 GpppAm in mRNA from mouse kidney (D), and NAD in total RNA from *E. coli* (E), showing HPLC elution profiles and MS/MS transitions (m/z X \rightarrow Y) for unlabeled pure standard (top), the RNA sample (middle), and isotope-labeled standard spiked into the RNA sample (bottom). Similar illustrations of CapQuant for all other caps are shown in Supplementary Figure S8.

aspects of mRNA fate and function, including mRNA stability and mRNA translation (2). In addition, the ribose 2'-O methylation (Nm) at the 5' penultimate nucleotide is thought to be a molecular signature that discriminates self and non-self mRNA, and thus functions in antiviral defense (3).

The family of eukaryotic RNA caps has recently expanded to include a variety of GpppX variants and non-canonical structures, such as the non-methylated guanosine cap (GpppN) in insect oocyte mRNA (4). Building on the m⁷GpppAm motif, Moss and colleagues showed that up to 30% of caps in animal and viral mRNAs are also methylated at N⁶ of Am (m⁶Am) (5). Multiple methylations also occur on the cap 5'-G, such as di- and tri-methylguanosine caps (e.g. m^{2,2,7}GpppN) in viral RNAs (6) and a subset of RNAP II-transcribed cellular RNAs, including small nuclear and nucleolar RNAs, and telomerase RNA (7). Perhaps the simplest methylated cap structure involves γ -phosphate methylation of unprocessed 5'-triphosphate (mPPPn) on small RNAs such as mammalian U6 and 7SK, mouse B2, and plant U3 RNAs (7).

A variety of non-canonical caps involving nucleotide metabolites (Figure 1A) have also recently been described (8,9). For example, nicotinamide adenine dinucleotide (NAD) and coenzyme A (CoA) were found as cap-like structures in bacterial small RNAs (10) and the NAD cap was also found in yeast and human mRNA and non-coding RNAs (11). Julius and Yuzenkova expanded the potential repertoire of caps by demonstrating that a variety of nucleotide metabolites could initiate transcription by bacterial RNA polymerase (RNA Pol) *in vitro*, including flavin adenine dinucleotide (FAD), uridine diphosphate glucose (UDP-Glc), and uridine diphosphate *N*-acetylglucosamine (UDP-GlcNAc) (9). They also showed that capping with NAD and UDP analogs by bacterial RNA Pol is promoter-specific and stimulates promoter escape (9), suggesting a role for metabolite caps in regulating gene expression. For example, the NAD cap has been shown to influence RNA stability and turnover, and is a substrate for decapping enzymes (11). However, the lack of sensitive and specific analytical methods has hindered the systematic study of the cap landscape dynamics in cells.

Analysis of RNA cap structures has traditionally relied on radioisotope labeling and enzymatic hydrolysis, followed by thin-layer and other types of chromatography to resolve cap structures (12–14). While sensitive, the radiolabeling approach lacks specificity (12) and has the potential to create cellular toxicity artifacts (15,16). While two-dimensional electrophoresis (14) allows multiple caps analysis, it (i) lacks specificity for identifying intact cap structures, (ii) is limited to NpppN caps, (iii) does not provide absolute quantification and (iv) is semi-quantitative at best. More recently, methods using high-pressure liquid chromatography (HPLC) with spectroscopic or mass spectrometry-based detection (LC–MS) have been developed (17–22). Though LC–MS provides chemical specificity, existing HPLC and LC–MS methods generally lack sensitivity and are not quantitative.

Here, we report a versatile and sensitive method for transcriptome-wide quantification of RNA caps—CapQuant—that combines off-line HPLC en-

richment of cap nucleotides with isotope-dilution, chromatography-coupled triple-quadrupole mass spectrometry (LC–MS/MS) to enable absolute quantification of any type of RNA cap structure with sensitivity (amol–fmol) and chemical specificity. Piloted with 26 different cap structures, this 'omic' approach provides important new insights into the landscape of RNA caps in cellular transcriptomes and viruses, and raises questions about current assumptions about cap biology.

MATERIALS AND METHODS

Cell and virus culture

CCRF-SB human B lymphoblasts (a gift from Dr Jianzhu Chen, Singapore-MIT Alliance for Research and Technology) were cultured in RPMI-1640 supplemented with 10% FBS, 50 μ g/ml streptomycin and 50 units/ml penicillin at 37°C and 5% CO₂. The cells were collected by centrifugation at 350 g for 10 min at 4°C. *Saccharomyces cerevisiae* strain W1588-4C (a gift from Dr Graham C. Walker, Massachusetts Institute of Technology) was grown exponentially in YPD medium (1% yeast extract, 2% peptone, 2% glucose) at 30°C with shaking at 200 rpm. *Escherichia coli* K-12 DH5 α cells were grown exponentially in LB broth at 37°C with shaking (220 rpm) to stationary phase. The cells were collected by centrifugation (4000 g at 4°C) and washed once with ice-cold PBS. All cells were stored at –80°C until total RNA extraction. The preparation and culture of DENV-2 strain TSV01 and isolation of the viral particles were conducted as described previously (23). Briefly, mosquito cells C6/36 were infected with DENV-2 strain TSV01 at an MOI (multiplicity of infection) of 0.1. The infected cells were incubated at 29°C for 5 days. The virus particles in cell culture supernatant were precipitated by adding 8% PEG8000 (w/v) and incubating the mixture overnight at 4°C. The precipitated virus particles were then resuspended in NTE buffer (120 mM NaCl, 12 mM Tris-HCl, 1 mM EDTA, pH 8.0) and concentrated by pelleting through a 24% (w/v) sucrose cushion at 75 000 g for 1.5 h at 4°C. The virus pellet was resuspended into 4% (w/v) potassium tartrate in NTE buffer and centrifuged at 149 000 g for 2 h at 4°C. The viruses were further purified by ultracentrifugation using a 10–30% (w/v) potassium tartrate gradient. The virus band was collected and concentrated using a 100 kDa centrifugal filter.

Mouse tissues

Three female C57BL/6 mice were bred in Comparative Medicine, National University of Singapore (NUS), following the policies and guidelines of the NUS Institutional Animal Care and Use Committee. The mice were sacrificed at 4–6 months of age for collection of tissues, which were snap-frozen in liquid nitrogen and stored at –80°C.

Cap nucleotide standards

GpppA, GpppG, m⁷GpppA and m⁷GpppG were purchased from New England Biolabs (NEB; Ipswich, MA, USA). NAD, FAD, UDP-Glc, UDP-GlcNAc and dp-CoA were purchased from Sigma Chemical Co. (St.

Louis, MO, USA). $m^{2,2,7}$ GpppG was purchased from Jena Bioscience (Jena, Thuringia, Germany). [$^{13}\text{C}_5$]- β -Nicotinamide adenine dinucleotide ammonium salt ($^{13}\text{C}_5$ -NAD) and [$^{13}\text{C}_5$]-flavin adenine dinucleotide ammonium salt hydrate ($^{13}\text{C}_5$ -FAD) were purchased from Medical Isotopes (Pelham, NH USA). [$^{13}\text{C}_6$]-Uridine diphosphate glucose ($^{13}\text{C}_6$ -UDP-Glc) disodium salt and uridine diphosphate *N*-acetylglucosamine- $^{13}\text{C}_6$ ($^{13}\text{C}_6$ -UDP-GlcNAc) disodium salt were from Omicron Biochemicals (South bend, IN, USA). GpppAm- and m^7 GpppAm-capped RNA oligos were synthesized by *in vitro* 2'-*O*-methylation of the penultimate adenosine residue of G-capped and m^7 G-capped dengue RNA representing the first 211 nucleotides of DENV-4 genome (strain MY-22713), respectively, by ScriptCap 2'-*O*-Methyltransferase. The dengue RNA was *in vitro* transcribed from PCR products amplified using an infectious cDNA clone as a template and the pairs of primer as below. Forward primer: 5'-CAGTAATACGAC TCACTATTAGTTGTTAGTCTGTGTGGAC-3', reverse primer: 5'-TAGCACCATCCGTAAGGGTC-3'. G-capped and m^7 G-capped RNA were generated using MEGAscript T7 Transcription Kit (Invitrogen) according to the manufacturer's instructions. Briefly, NTPs (ATP = 6 mM, GTP = 7.5 mM, CTP = 7.5 mM, UTP = 7.5 mM) and GpppA (1.5 mM) or m^7 GpppA (1.5 mM) were added into the reaction. Capped RNA was purified by passing through two G-25 size columns (GE Healthcare), extracted with phenol-chloroform, and precipitated with ethanol. The purified capped RNA was subjected to 2'-*O* methylation using ScriptCapTM 2'-*O*-methyltransferase (Epicentre) in the presence of cold *S*-adenosyl methionine (SAM) following the Instruction Manual. The methylated RNA oligos were purified in the same fashion as the capped RNA. RNA oligos (22 nt) with the following caps were synthesized by *in vitro* reaction of pppXGGCUCGAACU UAAUGAUGACG (Bio-Synthesis Inc., X = C, U, G, A, m^6 A, Cm, Um or Gm) with the Vaccinia Capping System (VCS) in the presence or absence of SAM, according to manufacturer directions: GpppC, GpppU, Gpppm⁶A, m^7 GpppC, m^7 GpppU, m^7 Gpppm⁶A, GpppCm, GpppUm, GpppGm, m^7 GpppCm, m^7 GpppUm and m^7 GpppGm. 500–1000 pmol of each pppXGGCUCGAACU UAAUGAUGACG RNA oligo was heated at 65°C for 5 min and then chilled on ice for 5 min. To the RNA was then added 10 μ l of 10 \times Capping Buffer (NEB), 5 μ l of 10 mM GTP, VCS (NEB, 50 U every two hours) and water, making a final volume of \sim 100 μ l. For the synthesis of m^7 GpppN and m^7 GpppNm, 20 mM of cold SAM (2 μ l per hour) was also added. The mixture was briefly mixed by vortexing and then incubated at 37°C for 4 h, with the enzyme subsequently removed by extraction with chloroform:isoamyl alcohol 24:1 (Sevag, Fluka). The RNA in the aqueous layer was then purified by passing through a 3000 Da spin filter, followed by washing three times with water. Gpppm⁶Am- and m^7 Gpppm⁶Am-capped RNA oligos were synthesized and purified as described previously (24). The synthesis and purification of RNA oligos with [$^{15}\text{N}_5$]-labeled G or m^7 G in the cap (GpppN, N = C, U, G, A or m^6 A; m^7 GpppN, N = C, U, G, A or m^6 A; GpppNm, Nm = Cm, Um, Gm or Am; and m^7 GpppNm, Nm = Cm, Um, Gm or

Am) were conducted with 200–500 pmol of each pppX GGCUCGAACU UAAUGAUGACG oligo as RNA substrate in the same fashion except that [$^{15}\text{N}_5$]-GTP (Sigma Chemical Co.) was used instead of GTP in the VCS reaction step. RNA oligo carrying a [$^{15}\text{N}_5$]- m^7 Gpppm⁶Am cap was synthesized as follows. Briefly, 500 pmol of RNA oligo pppm⁶AGGCUCGAACU UAAUGAUGACG (Bio-Synthesis Inc.; Lewisville, TX, USA) was heated at 65°C for 5 min and then chilled on ice for 5 min. To the RNA was then added 5 μ l of 10 \times Capping Buffer, 5 μ l of 10 mM GTP, 20 mM of cold SAM (2 μ l/h), VCS (20 U every 2 h), vaccinia mRNA 2'-*O*-methyltransferase (NEB, 250 U every 2 h) and water, making a final volume of \sim 50 μ l. The mixture was briefly mixed by vortexing and then incubated at 37°C for 4 h, with the enzymes subsequently removed by extraction with Sevag. The RNA in the aqueous layer was then purified in the same way as described above. RNA oligo carrying a [$^{15}\text{N}_5$]-Gpppm⁶Am cap was synthesized as follows. Briefly, 250 pmol of oligo pppm⁶AGGCUCGAACU UAAUGAUGACG (Bio-Synthesis Inc.; Lewisville, TX, USA) was heated at 65°C for 5 min and then chilled on ice for 5 min. To the RNA was then added 5 μ l of 10 \times Capping Buffer, 2.5 μ l of 10 mM [$^{15}\text{N}_5$]-GTP, 20 mM of cold SAM (1 μ l/h), VCS (10 U every two hours) and water, making a final volume of \sim 50 μ l. The mixture was briefly mixed by vortexing and then incubated at 37°C for 4 h, with the enzyme subsequently removed by extraction with Sevag. The RNA in the aqueous layer was purified in the same way as described above. The purified RNA was heated at 65°C for 5 min and then chilled on ice for 5 min. To the RNA was then added 10 μ l of 400 mM Tris-HCl pH 7.5, 10 μ l of 50 mM DTT, 20 mM of cold SAM (2 μ l/h), DENV NS5 methyltransferase (200 pmol every 2 h) and water, making a final volume of \sim 100 μ l. The mixture was briefly mixed by vortexing and then incubated at 37°C for 4 h, with the enzyme subsequently removed by extraction with Sevag. The RNA in the aqueous layer was purified in the same way as described above. All synthetic capped oligos were digested with NP1 (30 mM sodium acetate pH 5.5 and 1 mM ZnCl_2 , 37°C) and the caps purified by ion-pairing HPLC, with cap fractions concentrated and cleaned up by Speed-vac, as described in the HPLC section below. All purified synthetic cap dinucleotides were >99% or >98% pure based on HPLC and were characterized by high-resolution mass spectrometry (HRMS) (Supplementary Table S1) and MS/MS analyses (Supplementary Figure S1). The synthesis of RNA oligo containing a mixture of m^7 Gpppm¹A and m^7 Gpppm¹Am in the 5' cap and the release and purification of m^7 Gpppm¹A and m^7 Gpppm¹Am were conducted in the same fashion. The purified m^7 Gpppm¹A and m^7 Gpppm¹Am were >98% and >99% pure respectively based on HPLC, with their identity confirmed by MS/MS analysis (Supplementary Figure S1) and successful detection of m^1 A and m^1 Am, but not m^6 A and m^6 Am, respectively by LC-MS/MS (Supplementary Figure S2) using the same method as the LC-MS/MS method described below for Dimroth rearrangement analysis following hydrolysis into nucleosides by RNA 5' pyrophosphohydrolase (RppH, NEB) and shrimp alkaline phosphatase (SAP, NEB). The concentrations of the caps, m^7 Gpppm¹A and m^7 Gpppm¹Am were measured by

their UV absorbance at 260 nm. The isotopic purity of the caps was found to be better than 99.6% (data not shown) based on LC–MS/MS analyses.

m¹A, m⁶A, m¹Am and m⁶Am nucleoside standards

m¹A, m⁶A and m⁶Am were purchased from Berry and Associates (Dexter, MI, USA). m¹Am was synthesized by reaction of methyl iodide (0.3 ml) with 2'-*O*-methyladenosine (100 mg) in anhydrous DMF (2.0 ml) in a closed flask with stirring at ambient temperature for 18 h. The reaction mixture was evaporated under vacuum and triturated with diethyl ether to afford a white solid (120 mg). A portion of this crude solid (40 mg) was dissolved in 3.0 ml of methanol and treated with aqueous ammonia (3.0 ml) by stirring at ambient temperature for 10 min. Following evaporation of solvent under vacuum, the mixture was resolved by chromatography on 200–400 mesh silica gel eluted with 15–20% methanol in dichloromethane with 1% aqueous ammonia to afford m¹Am (25 mg, 59%) as a white solid. The product was characterized by ¹H and ¹³C NMR (Supplementary Figure S3) and HRMS: ¹H NMR (DMSO-*D*₆, 400 MHz) δ 8.18 (s, 1H), 8.09 (s, 1H), 7.03 (bs, 1H), 5.87 (d, *J* = 6.00 Hz, 1H), 5.25 (d, *J* = 5.24 Hz, 1H), 5.14 (t, *J* = 5.54 Hz, 1H), 4.29 (m, 1H), 4.25 (m, 1H), 3.95 (q, *J* = 10.68 Hz, 1H), 3.65 (m, 1H), 3.56 (m, 1H), 3.43 (s, 3H), 3.31 (s, 3H); ¹³C (DMSO-*D*₆, 100 MHz) δ 154.8, 149.1, 141.9, 138.1, 123.1, 86.7, 85.9, 83.4, 69.1, 61.8, 58.0, 35.1; HRMS (ESI, *m/z*) calculated for C₁₂H₁₈N₅O₄ [M+H]⁺: 296.1359, found: 296.1370, mass error <5 ppm.

H₂O₂ and MMS treatment

Treatment of *S. cerevisiae* W1588-4C cells with 6 mM of MMS or 2 mM of H₂O₂ was started when the O.D. reached ~0.5. After 1 h treatment, the cells were collected by centrifugation (4500 g at 4°C) and washed twice with ice-cold PBS.

RNA extraction

The total RNA from CCRF-SB pellets was directly extracted with TRIzol reagent (Life Technologies), according to the manufacturer's protocol. For mice, the liver and kidney tissues were ground under liquid nitrogen into fine powders in a mortar, the total RNA of which were then extracted with TRIzol reagent as described earlier. For yeast, total RNA was extracted with a MasterPure Yeast RNA Purification kit (Epicentre) following the manufacturer's protocol. For *E. coli*, lysis was performed with lysozyme, before total RNA was extracted with TRIzol reagent as described earlier. Briefly, 0.8 ml of TE buffer (pH 8.0) containing 80 mg lysozyme (Fluka) was added to approximately 3.7 × 10¹⁰ *E. coli* DH5α cells and the mixture was incubated for 2 h at room temperature. To the mixture was then added 0.6 ml of TE buffer (pH 8.0) containing 60 mg lysozyme, followed by incubation for another 2 h at room temperature. Total RNA was subsequently extracted with TRIzol following the manufacturer's instructions. The genomic RNA from purified dengue virions was extracted with TRIzol and

purified by size-exclusion chromatography as described previously (23,25). The poly(A)-tailed RNA in human CCRF-SB cells was isolated from the total RNA using a Fast-track MAG Maxi mRNA isolation kit (Life Technologies), whereas the poly(A)-tailed RNA in yeast cells and mouse tissues was isolated from the total RNA using a Dynabeads mRNA Purification kit (Life Technologies) following the manufacturer's protocols. rRNA depletion of the poly(A)-tailed RNA isolated from yeast cells and mouse tissues was subsequently performed using a GeneRead rRNA Depletion kit (Qiagen), according to the manufacturer's protocol. The rRNA-depleted RNA was then cleaned up using a RNeasy MinElute Cleanup kit (Qiagen), following the manufacturer's protocol. No rRNA depletion and subsequent clean-up was performed for the poly(A)-tailed RNA isolated from human CCRF-SB cells because there was no sign of significant rRNA contamination (Supplementary Figure S4). All RNA samples were stored at –80°C before use. The quality of the total RNA (Supplementary Figure S5), poly(A)-tailed RNA (Supplementary Figure S4), and purified DENV-2 RNA genome (Supplementary Figure S4) was assessed using an Agilent Bioanalyzer (Agilent Technologies) with RNA 6000 Nano or Pico chips.

RNA hydrolysis

Isolated RNA (200 μg for total RNA and 0.6–7.8 μg for mRNA and RNA genome) was incubated with NP1 (1 unit/μg RNA, Sigma) in a solution containing 30 mM sodium acetate pH 5.5, 1 mM ZnCl₂ and 24 SIL-CNs at 37°C for 1 h. These SIL-CNs included 200 fmol of NAD, 200 fmol of FAD, 500 fmol of UDP-Glc, 500 fmol of UDP-GlcNAc, 500 fmol of GpppC, 200 fmol of GpppU, 400 fmol of GpppG, 500 fmol of GpppA, 500 fmol of Gpppm⁶A, 500 fmol of m⁷GpppC, 200 fmol of m⁷GpppU, 1000 fmol of m⁷GpppG, 500 fmol of m⁷GpppA, 100 fmol of m⁷Gpppm⁶A, 1000 fmol of GpppCm, 200 fmol of GpppUm, 1000 fmol of GpppGm, 500 fmol of GpppAm, 100 fmol of Gpppm⁶Am, 500 fmol of m⁷GpppCm, 200 fmol of m⁷GpppUm, 500 fmol of m⁷GpppGm, 500 fmol of m⁷GpppAm and 200 fmol of m⁷Gpppm⁶Am. The enzyme was subsequently removed by extraction with Sevag. The resulting aqueous layer was subjected to off-line HPLC separation for the enrichment of the CNs and their analogs (m⁷Gpppm¹A and m⁷Gpppm¹Am) under study.

HPLC

A 4.6 mm × 250 mm Alltima HP C18 column (5 μm in particle size, Hichrom) was used for the enrichment of CNs and their analogs from the enzymatic digestion products of RNA. A solution of 10 mM dibutylammonium acetate (DBAA) in 5% ACN-95% H₂O (solution A) and 10 mM DBAA in 84% ACN-16% H₂O (solution B) were used as mobile phases, and the flow rate was 0.8 ml/min. A gradient of 20 min 0% B and 40 min 0–40% B was employed. A typical HPLC trace is depicted in Figure 1C. The HPLC fractions eluting approximately at 10.0–12.0, 13.5–15.9, 19.0–20.6, 23.0–28.0, 32.0–36.0, 36.0–37.5, 37.5–39.0, 39.0–41.5, 41.5–43.0 and 43.0–46.5 min were pooled for NAD, m⁷Gpppm¹A, m⁷Gpppm¹Am, (UDP-Glc and

UDP-GlcNAc), (m^7 GpppC, m^7 GpppU, m^7 GpppG and m^7 GpppCm), (GpppC, GpppU, GpppG, m^7 GpppA and m^7 GpppUm), (GpppA, Gpppm⁶A, m^7 Gpppm⁶A, m^7 GpppGm, m^7 GpppAm, $m^{2,2,7}$ GpppG and dpCoA), (FAD, GpppCm and m^7 Gpppm⁶Am) and (GpppUm, GpppAm, GpppGm and Gpppm⁶Am), respectively. The collected fractions were dried in the Speed-vac, reconstituted in acetonitrile:water 3:7 (v/v) and dried for three cycles to remove the ion-pairing reagent present in the fractions, reconstituted in 8 mM ammonium bicarbonate pH 7.0 (solution C), and injected for LC-MS/MS analysis.

LC-MS/MS analysis of cap nucleotides

Using purchased and synthetic standards, we defined the HPLC retention times for the 26 CNs and two analogs of them (m^7 Gpppm¹A and m^7 Gpppm¹Am) on a Luna Omega PS C18 column (100 × 2.1 mm, 1.6 μm) coupled to an Agilent 1290 HPLC system and an Agilent 6460 triple quad mass spectrometer. The elution was conducted at 15°C and a flow rate of 200 μl/min, with a gradient of 100% solution C and 0% solution D (methanol) for 5 min, followed by 0–48% solution D over a period of 12 min. The HPLC column was coupled to an Agilent 6460 Triple Quad mass spectrometer with an electrospray ionization source in positive or negative mode with the following parameters: gas temperature, 350°C; gas flow, 11 l/min; nebulizer, 20 psi; sheath gas temperature, 300°C; sheath gas flow, 12 l/min; capillary voltage, 1800 V; nozzle voltage, 2000 V; fragmentor voltage, 135 V; ΔEMV, 400 V. MRM mode was used for detection of product ions derived from the precursor ions for all the 26 unlabeled CNs and 24 SIL-CN with instrument parameters which mainly included the collision energy (CE) optimized for maximal sensitivity for the CNs (mode, retention time in min, precursor ion of unlabeled CN m/z , product ion(s) of unlabeled CN m/z (CE), precursor ion of labeled CN m/z , product ion of labeled CN m/z (CE)): NAD, positive, 9.3, 664, 136 (39 V), 232 (24 V), 428 (30 V), 669, 136 (39 V); FAD, positive, 14.0, 787, 348 (20 V), 136 (44 V), 439 (28 V), 782, 353 (20 V); UDP-Glc, negative, 1.3, 565, 323 (24 V), 79 (76 V), 211 (32 V), 570, 323 (24 V); UDP-GlcNAc, negative, 1.4, 606, 385 (28 V), 273 (36 V), 282 (36 V), 612, 385 (28 V); GpppC, positive, 1.7, 749, 152 (60 V), 754, 157 (60 V); GpppU, positive, 2.0, 750, 152 (28 V), 755, 157 (28 V); GpppG, positive, 2.2, 789, 152 (60 V), 794, 157 (60 V); GpppA, positive, 3.9, 773, 136 (56 V), 778, 136 (56 V); Gpppm⁶A, positive, 8.8, 787, 150 (80 V), 792, 150 (80 V); m^7 GpppC, positive, 1.8, 763, 166 (56 V), 768, 171 (56 V); m^7 GpppU, positive, 1.8, 764, 166 (36 V), 769, 171 (36 V); m^7 GpppG, positive, 5.4, 803, 248 (32 V), 808, 248 (32 V); m^7 GpppA, positive, 10.8, 787, 136 (68 V), 792, 136 (68 V); m^7 Gpppm⁶A, positive, 9.3, 801, 150 (80 V), 806, 150 (80 V); GpppCm, positive, 2.3, 763, 111 (52 V), 768, 111 (52 V); GpppUm, positive, 3.7, 764, 152 (40 V), 769, 157 (40 V); GpppGm, positive, 8.2, 803, 111 (56 V), 808, 111 (56 V); GpppAm, positive, 8.8, 787, 136 (60 V), 792, 136 (60 V); Gpppm⁶Am, positive, 10.2, 801, 150 (72 V), 806, 150 (72 V); m^7 GpppCm, positive, 3.4, 777, 166 (52 V), 782, 171 (52 V); m^7 GpppUm, positive, 6.2, 778, 166 (32 V), 783, 171 (32 V); m^7 GpppGm, positive, 8.5, 817, 166 (68 V), 822, 171 (68

V); m^7 GpppAm, positive, 9.7, 801, 136 (68 V), 806, 136 (68 V); m^7 Gpppm⁶Am, positive, 10.8, 815, 150 (76 V), 820, 150 (76 V); dpCoA, positive, 11.7, 689, 261 (24 V), 348 (20 V), 136 (40 V); $m^{2,2,7}$ GpppG, positive, 8.5, 831, 194 (64 V), 248 (28 V), 566 (32 V); m^7 Gpppm¹A, positive, 4.2, 401, 166 (16 V), 150 (36 V); m^7 Gpppm¹Am, positive, 9.3, 408, 166 (16 V), 150 (32 V), 111 (36 V).

Genome-wide nucleotide distribution of TSS

To cross-validate the CapQuant results obtained in this study, transcriptional start site (TSS) nucleotide identities were mined from the 5' terminal positions of capped transcripts mapped using cap-analysis gene expression (CAGE) approach (26,27). CAGE datasets were chosen over others, such as serial analysis of gene expression, as the CAGE method captures mRNA transcripts at the 7-methylguanosine cap to pulldown the 5'-cDNAs reversely transcribed from them (28) for subsequent tagging and high-throughput sequencing. It achieves genome-wide 1bp-resolution map of TSSs and expression levels. Mapped TSS reads are represented as units of peaks due to varying spread of positions which have first base signals within a promoter, and a reading of greater than 10 read counts and 1 tag per million (TPM) signifies a robust TSS signal. The TSS analysis workflow herein is outlined in Supplementary Figure S6a. CAGE data in .bedgraph format for *Sacharromyces cerevisiae* BY4741 was obtained from the YeastTSS Atlas (Yeast Transcription Start Site Atlas) (29). While CAGE data for human and mouse was obtained from the FANTOM5 project (Functional ANnotation Of Mammalian genomes) via <http://fantom.gsc.riken.jp/5/datafiles/reprocessed/> (30,31). These datasets were uploaded into the main public Galaxy server (32) into separate history list with the referent genome set to the latest assembly for further processing. First, non-robust TSS signals were removed in yeast data (c4 of .bedgraph file), a score of > 1 and < -1 was filtered for the positive and negative strand respectively. Second, GetFastaBed under BedTools (33) was used to extract the respective TSS nucleotide information in tab-delimited format and force strandedness applied to reverse complement negative sense strand. GetFastaBed for human and mouse data were obtained from thickStart and thickEnd (c7 and c8) positions, Trimmed up to position 1 to obtain the 5' terminal nucleotide only, Change Case to upper case. Third, Count under Statistics to obtain the TSS nucleotide distribution histograms for human (Supplementary Figure S6b), mouse (Supplementary Figure S6c), and yeast data (Supplementary Figure S6d). As the number of transcripts generated from different TSSs can be very different, the weighted and unweighted nucleotide frequency of TSS could affect correlation accuracy. To account for the weight of TSS usage frequency according to transcript abundance, Datamash was performed by grouping the nucleotides together and summing the CTSS read counts (c5 of .bed file) to obtain the weighted values for human (Supplementary Figure S6b), mouse (Supplementary Figure S6c) and yeast (Supplementary Figure S6d). The work histories can be accessed via https://usegalaxy.org/histories/list_published?f-username=alvin-chew

Dimroth rearrangement

Due to the limited quantities of $m^7\text{Gpppm}^1\text{A}$ and $m^7\text{Gpppm}^1\text{Am}$ we obtained, we performed the testing of the Dimroth rearrangement with purchased $m^1\text{A}$ and synthetic $m^1\text{Am}$ nucleoside standards (Supplementary Figure S7). Because the CCRF-SB mRNA samples were the most abundant mammalian mRNA samples we had and they were the only mRNA samples for which no further purification by rRNA depletion was performed, we chose to use the CCRF-SB mRNA samples for the analysis. We treated a mixture of $m^1\text{A}$ and $m^1\text{Am}$ in the same fashion as CCRF-SB cells or the isolated RNA as we went through the RNA extraction, purification, cleanup and enzymatic digestion steps (Supplementary Figure S7a) as described above. The $m^1\text{A}$, $m^6\text{A}$, $m^1\text{Am}$ and $m^6\text{Am}$ in the samples were separated on a Hypersil GOLD aQ C18 column (100 × 1 mm, 1.9 μm) coupled to an Agilent 1290 HPLC system and an Agilent 6460 triple quad mass spectrometer. The elution was conducted at 24°C and a flow rate of 100 μl/min, with a gradient of 100% solution E (0.1% formic acid in water) to 89% solution E-11% solution F (0.1% formic acid in acetonitrile) over a period of 11 min, followed by a gradient of 11% to 80% solution F over a period of 3 min. The HPLC column was coupled to an Agilent 6460 Triple Quad mass spectrometer with an electrospray ionization source in positive mode with the following parameters: gas temperature, 300°C; gas flow, 5 l/min; nebulizer, 45 psi; sheath gas temperature, 200°C; sheath gas flow, 5 l/min; capillary voltage, 3,500 V; nozzle voltage, 500 V; fragmentor voltage, 110 V; ΔEMV, 800 V. MRM mode was used for detection of product ions derived from the precursor ions for $m^1\text{A}$, $m^6\text{A}$, $m^1\text{Am}$ and $m^6\text{Am}$ with the following instrument parameters (retention time in min, precursor ion m/z , product ion m/z , CE): $m^1\text{A}$, 2.4, 282, 150, 15 V; $m^6\text{A}$, 6.1, 282, 150, 15 V; $m^1\text{Am}$, 4.5, 296, 150, 15 V; $m^6\text{Am}$, 7.8, 296, 150, 15 V.

Quantitative real-time PCR

Quantitative real-time PCR (RT-qPCR) was performed to assess the relative mRNA abundance of a selection of RNA cap modification enzymes in human and mouse cells, including PCIF1 (the enzyme responsible for the synthesis of $m^6\text{Am}$ in mRNA caps), FTO (an RNA N^6 -methyladenine demethylase that can act on cap $m^6\text{A}/m^6\text{Am}$ in mammals), DCP2 (a major RNA decapping enzyme in mammals) and CMTR1 (cap 1 2'-*O*-ribose methyltransferase), as well as ALKBH5 (another RNA N^6 -methyladenine demethylase) in the total RNA from CCRF-SB cells and mouse liver and kidney tissues. Using primers listed in Supplementary Table S2, total RNA (1 μg) was reverse transcribed using iScript cDNA Synthesis Kit (Bio-Rad) according to the manufacturer's instructions. The cDNA was subjected to qPCR analysis using BlitzAmp qPCR Master Mix (MiRXES Pte. Ltd.) according to the manufacturer's fast thermal cycling instructions on a CFX96 Realtime-PCR System (Bio-Rad). Experiments were performed with three biological and two technical replicates in hard-shell thin wall PCR plates (#HSP9601; Bio-Rad). No template and no reverse transcriptase controls were used to assess primer dimerization and genomic DNA contamination, respectively. Relative gene expression was calculated using a modified com-

parative method for geometric averaging of two reference genes, Gapdh and Polr2a, for more reliable normalization (34). Data visualization and Student's t-test statistical analysis was performed using Graphpad Prism software (version 8.0).

RESULTS

Development of CapQuant

The workflow for CapQuant (Figure 1B) uses nuclease P1 (NP1) to hydrolyze RNA to nucleoside monophosphates (NMPs) while sparing di- and tri-phosphate linkages that characterize the NpppN and NppN caps (24,35). Following removal of NP1, cap structures and 5'-NMPs in the limit digest are resolved by reversed-phase ion-pairing HPLC (Figure 1C) and cap-containing fractions isolated for subsequent LC-MS/MS quantification. Here we targeted 26 caps that embraced a variety of known and possible structures: $m^7\text{GpppN}$, $m^7\text{GpppNm}$, GpppN, GpppNm (N = C, U, G, A or $m^6\text{A}$), and NAD, FAD, UDP-Glc, UDP-GlcNAc, $m^{2,2,7}\text{GpppG}$ and dpCoA. The 26 caps were well resolved from 5'-NMPs (Figure 1C), separating each member of four isobaric pairs using mobile phases containing the volatile ion-pairing reagent dibutylammonium acetate (DBAA). Cap-containing fractions were collected and the volatile ion-pairing agent completely removed by three cycles of drying and reconstitution in acetonitrile:water 3:7 (v/v). Samples were finally reconstituted in ammonium bicarbonate buffer (pH 7.0) for subsequent analysis.

Individual caps were next quantified by isotope-dilution LC-MS/MS, the most rigorous approach for sensitivity, specificity, and quantitative accuracy. HPLC conditions for the LC-MS/MS analysis were systematically optimized using standards for the 26 caps, with assessment of different solid phases (C18/NH₂ reversed-phase, HILIC, porous graphite), pH values (2.7–9.0), and column temperatures (10–45°C). The best overall resolution and sensitivity were obtained with a positive-surface C18 column at 15°C with volatile ammonium bicarbonate (pH 7.0) as a mobile phase. Isotope-labeled standards for 24 of the 26 caps were spiked into RNA samples prior to NP1 hydrolysis and each cap was identified by HPLC retention time and collision-induced dissociation (CID) patterns, using MS parameters optimized for each cap (Figure 1D and E; Supplementary Figure S8). Quantification was achieved using a calibration curve for each cap (Supplementary Figure S9) generated by multiple-reaction monitoring (MRM), with one MRM transition for $m^7\text{GpppN}$, $m^7\text{GpppNm}$, GpppN and GpppNm caps and three MRM transitions for the other six caps (Figure 1D and E, Supplementary Figure S8). This resulted in limits of detection (LODs) ranging from 19 amol to 13 fmol for 23 caps, and up to 160 fmol for three caps (GpppC, GpppCm and GpppGm; Supplementary Table S3). As shown in Figure 1D and E, which depicts applications of the method to mouse (C57BL/6) kidney mRNA and *E. coli* DH5α total RNA, CapQuant proved to be sensitive, precise, and accurate.

Using this new method, control experiments were performed to ensure complete cap release and stability during sample processing. To confirm that all detected caps were indeed covalently linked to mRNA prior to NP1 digestion

and not present as contaminants, we used the method to analyze *S. cerevisiae* mRNA and *E. coli* total RNA except that NP1 was removed from its stock solution with a 3000 Da filter and the filtrate used in the RNA digestion reaction. None of the cap analytes were detectable in subsequent LC–MS/MS analyses, from which we conclude that CapQuant analytes are truly RNA caps. To validate complete and unbiased release of all m⁷G caps from RNA, we quantified release of m⁷GpppN and m⁷GpppNm (N = C, U, G, A or m⁶A) from synthetic oligonucleotides, with the results showing quantitative release of all m⁷GpppN and m⁷GpppNm caps (Supplementary Figure S10). Finally, the stability of cap structures during NP1 digestion was verified by spiking cap standards into the RNA digestion reactions with subsequent HPLC purification and isotope-dilution LC–MS/MS analysis (Figure 1D and E).

Recently a new type of mRNA cap has been proposed containing m¹A (36–38). These caps, m⁷Gpppm¹A or m⁷Gpppm¹Am, were predicted based on the binding of m¹A antibodies to 5' ends of mRNA (39). However, no biochemical validation was presented. To quantify these caps biochemically, we first wanted to develop cap purification protocols that would preserve m¹A, due to the potential for this nucleotide to convert to m⁶A by the Dimroth rearrangement (Supplementary Figure S7a) (36–38), we defined the fate of m¹A and m¹Am ribonucleosides during the RNA isolation and processing. As shown in Supplementary Figure S7b, conversion of m¹A to m⁶A occurred at each step—TRIZOL RNA extraction (7%), polyA-tailed RNA purification (17%), GeneRead rRNA depletion (36%), and RNeasy MinElute Cleanup (72%). This means that for yeast and mouse RNA, which were processed with all steps, 86% of initial m¹A would have been converted to m⁶A. With LODs of 0.68 fmol for m⁷Gpppm¹A and 0.11 fmol for m⁷Gpppm¹Am (Supplementary Table S3), m¹A- and m¹Am-containing caps present at 10 fmol per μg of RNA, which is the lowest level among all of the canonical caps in humans, mice, and yeast as discussed shortly, would remain detectable even with 90% loss caused by adventitious Dimroth rearrangement. For human RNA, which was processed without rRNA depletion and the RNA cleanup steps, m¹A and m¹Am losses were at most 23%, so m⁷Gpppm¹A and m⁷Gpppm¹Am should be readily detectable in human mRNA if present.

Based on our validation steps, CapQuant was now applied to viral, bacterial, yeast, mouse, and human RNA to discover new cap structures, quantify m¹A or m¹Am in caps, and to define the composition and dynamics of the cap epitranscriptome.

Quantitative analysis of the cap landscape in eukaryotic, prokaryotic, and viral RNA

With an optimized CapQuant method in hand, we applied it to define the landscape of caps in coding and non-coding RNAs from a range of organisms, including humans, mice, yeast, bacteria, and an RNA virus. Focusing first on poly(A)-tailed RNAs (mainly mRNA) from log-growing human CCRF-SB lymphoblasts (Figure 2A), we were able to quantify the components of the cap epitranscriptome. Of the 26 targeted caps, 10 were reproducibly de-

tected for a total of 2078 fmol of caps per μg of RNA. As expected, the five cap 1 structures (m⁷GpppNm) comprised the majority of all caps (88%, 1830 fmol/μg RNA) with no cap 0 structures (m⁷GpppN) detected. Consistent with the fact that very few TSS in humans start with a uridine (Figure 3A and Supplementary Figure S6b), m⁷GpppUm comprised only 1% of second-nucleotide subtypes (Figure 2A), which ranged from 23 to 595 fmol/μg RNA. The most abundant caps were the C, G and A subtypes, found in nearly equal proportions: 33% m⁷GpppCm, 32% m⁷GpppGm, and 19% m⁷Gpppm⁶Am/15% m⁷GpppAm. This distribution correlates strongly with the distribution of predicted TSS (+1 position) frequencies in humans (Figure 3A and Supplementary Figure S6b). Our analysis further revealed four previously undescribed cap structures (Figure 1A): m⁷Gpppm⁶A, FAD, UDP-Glc, and UDP-GlcNAc. The m⁷Gpppm⁶A structure proved to be relatively abundant at 12% of all mRNA caps (244 fmol/μg RNA), which contradicts previous claims of the absence of this cap based on crude thin-layer chromatography analyses (14) and in a non-quantitative LC–MS assay (18). Additionally, this cap demonstrates that 2'-O-methylation is not essential in mRNAs, as has been previously suggested to suppress innate host antiviral responses (3). The structures of the four metabolite caps (NAD, FAD, UDP-Glc and UDP-GlcNAc) were unequivocally confirmed by three signature MRM transitions defined with standards (Figure 1E and Supplementary Figure S8). Compared to cap 1 structures, however, the levels of these metabolite caps were ~100-fold lower at 0.40–2.9 fmol/μg RNA (Figure 2A and Table 1). UDP-GlcNAc and NAD being the two most abundant structures is consistent with the relative abundance of these metabolites in human cells (40,41) and thus with the idea that nucleotide metabolites can initiate transcription (9). Notably, we were unable to detect m⁷Gpppm¹A or m⁷Gpppm¹Am in human mRNAs (Supplementary Figure S11).

We next sought to understand whether the cap epitranscriptome differs among cell types. The same 10 mRNA caps observed in the human cells were also found in mouse liver and kidney tissue mRNAs at 1131 and 566 fmol/μg RNA, respectively. Mice similarly showed relatively low abundance of m⁷GpppUm and high levels of m⁷GpppGm and m⁷GpppCm (Figure 2B and Table 1), though m⁷GpppAm was >5-fold lower in mice liver and kidney than in human CCRF-SB cells (Figure 2B and Table 1). The large differences between the ratio of m⁷GpppAm and m⁷Gpppm⁶Am in different cell types supports a role for m⁶Am as a regulatable modification in mRNA. A comparison of caps in liver and kidney showed several striking tissue-specific differences, most notably the absence of detectable m⁷Gpppm⁶A in kidney (Figure 2B and Table 1). Other tissue-specific differences include >2-fold lower levels of m⁷GpppGm ($P > 0.05$), m⁷GpppAm ($P > 0.05$), m⁷Gpppm⁶Am ($P < 0.05$) and UDP-Glc ($P < 0.01$) in kidney compared to liver, and small variations in the levels of m⁷GpppCm, m⁷GpppUm, NAD, FAD and UDP-GlcNAc (Figure 2B). Similar to humans, the cap second nucleotide distribution correlates strongly with the distribution of predicted TSS frequencies in mice (Figure 3B and Supplementary Figure S6c).

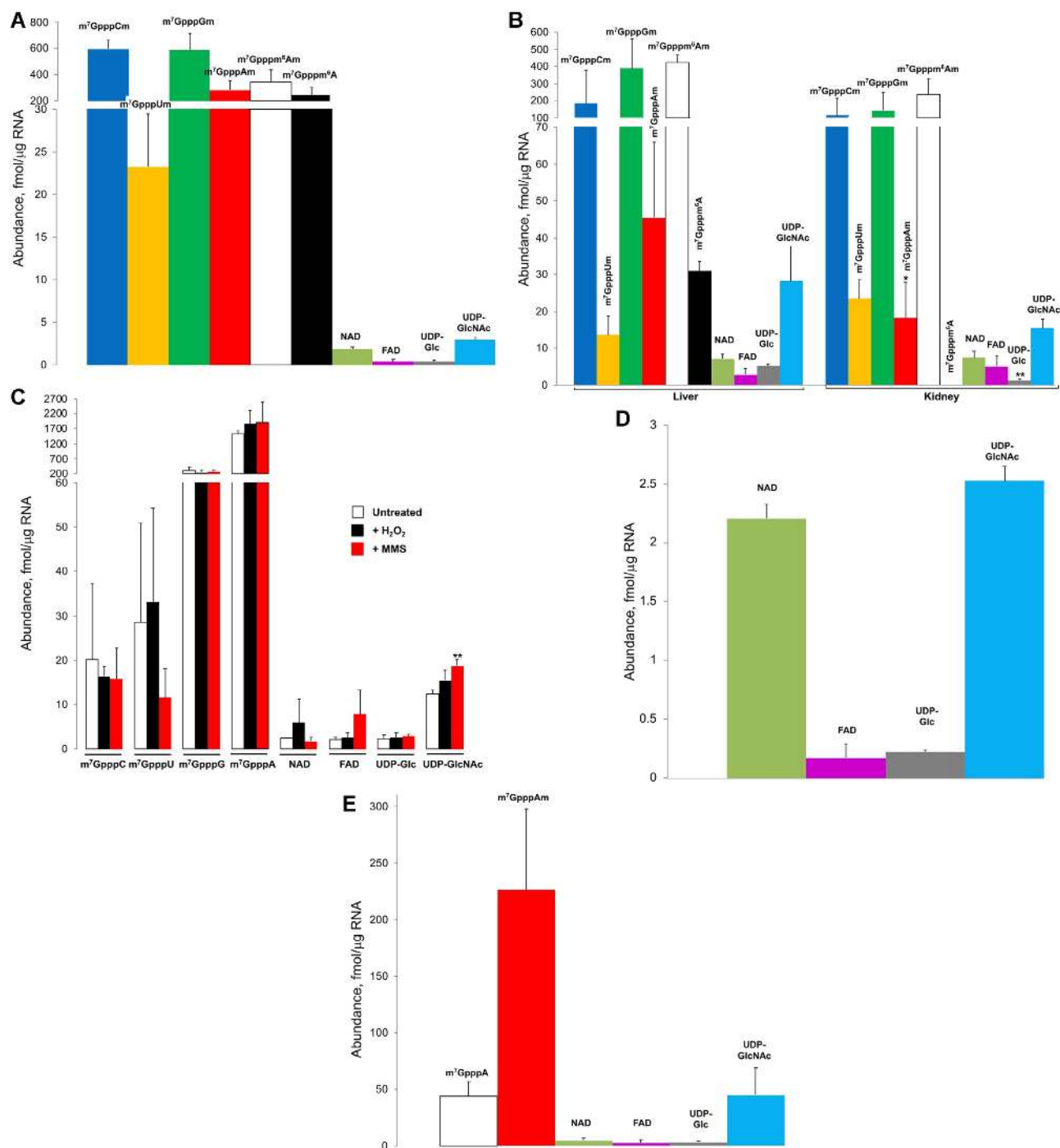


Figure 2. Quantification of 5' cap structures in cellular RNA and viral RNA genome by CapQuant. (A) mRNA from Human CCRF-SB cells. (B) mRNA from mouse C57BL/6 liver and kidney tissues. * $P < 0.05$, ** $P < 0.01$, two-tailed paired Student's t test. (C) mRNA from *Saccharomyces cerevisiae* W1588-4C cells. Exposure to hydrogen peroxide (H₂O₂) or methyl methanesulfonate (MMS) induces changes to the profile of 5' cap structures in mRNA from *Saccharomyces cerevisiae*. From left to right: untreated, H₂O₂-treated, MMS-treated. ** $P < 0.01$, two-tailed unpaired Student's t test. (D) *E. coli* DH5α total RNA. (E) DENV-2 virus RNA genome. Values represent mean \pm SD for three independent cultures for CCRF-SB, W1588-4C and DH5α, for three biological replicates of three mice and H₂O₂- or MMS-treated W1588-4C cells, and for three technical replicates of a single culture for DENV-2.

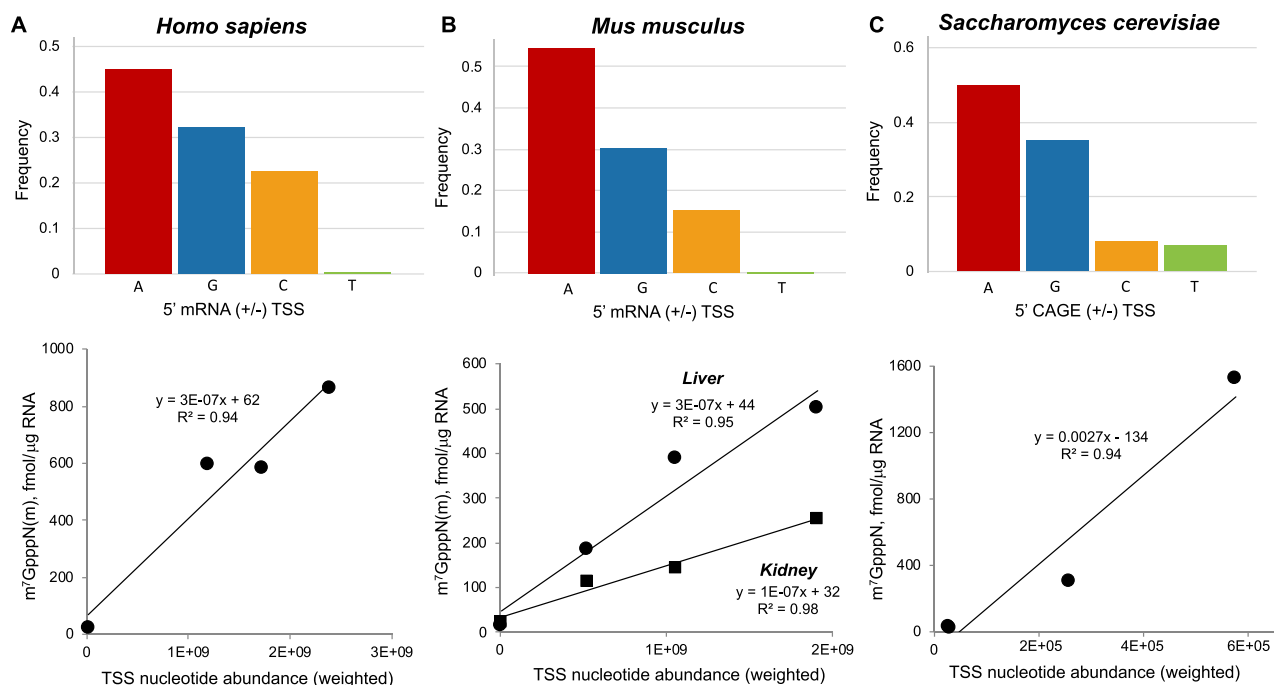


Figure 3. Cap profile correlation with CAGE-analyzed transcription start site (TSS) nucleotide distribution. The frequency of A, G, C and T as the second nucleotide in m^7 GpppN caps was plotted against the distribution of these nucleotides at TSSs in (A) human (FANTOM5-weighted TSS), (B) mouse liver and kidney (FANTOM5-weighted TSS) and (C) *Saccharomyces cerevisiae* (YeastTSS-weighted TSS). TSS values were calculated as described in MATERIALS AND METHODS.

Table 1. Cap compositions in cellular and viral RNA species^a

Cap	Level, fmol per μ g RNA					
	(Percentage, %)					
	Human CCRF-SB mRNA	Mouse C57BL/6 liver mRNA	Mouse C57BL/6 kidney mRNA	<i>S. cerevisiae</i> W1588-4C mRNA	<i>E. coli</i> DH5 α total RNA	DENV-2 TSV01 RNA genome
m^7 GpppCm	595 \pm 65 (27 \pm 3)	184 \pm 195 (16 \pm 17)	114 \pm 101 (20 \pm 18)	nd	nd	nd
m^7 GpppUm	23 \pm 6 (1.1 \pm 0.3)	14 \pm 5 (1.2 \pm 0.5)	24 \pm 5 (4.2 \pm 0.9)	nd	nd	nd
m^7 GpppGm	585 \pm 128 (28 \pm 6)	389 \pm 172 (34 \pm 15)	144 \pm 105 (25 \pm 18)	nd	nd	nd
m^7 GpppAm	282 \pm 76 (14 \pm 4)	46 \pm 20 (4.0 \pm 1.8)	18 \pm 10 (3 \pm 2)	nd	nd	226 \pm 72 (70 \pm 22)
m^7 Gpppm ⁶ Am	345 \pm 93 (17 \pm 4)	425 \pm 43.4 (38 \pm 4)	237 \pm 92 (42 \pm 16)	nd	nd	nd
m^7 GpppC	nd	nd	nd	20 \pm 17 (1.1 \pm 0.9)	nd	nd
m^7 GpppU	nd	nd	nd	28 \pm 22 (1.5 \pm 1.2)	nd	nd
m^7 GpppG	nd	nd	nd	305 \pm 130 (16 \pm 7)	nd	nd
m^7 GpppA	nd	nd	nd	1524 \pm 106 (80 \pm 6)	nd	44 \pm 12 (14 \pm 4)
m^7 Gpppm ⁶ A	244 \pm 61 (12 \pm 3)	31 \pm 3 (2.7 \pm 0.2)	nd	nd	nd	nd
NAD	1.9 \pm 0.2 (0.09 \pm 0.01)	7.1 \pm 1.2 (0.6 \pm 0.1)	7.4 \pm 1.8 (1.3 \pm 0.3)	2.4 \pm 0.1 (0.13 \pm 0.01)	2.2 \pm 0.1 (43 \pm 2)	4.5 \pm 2.5 (1.4 \pm 0.8)
FAD	0.4 \pm 0.2 (0.02 \pm 0.01)	2.8 \pm 1.8 (0.2 \pm 0.2)	5.0 \pm 3.1 (0.9 \pm 0.5)	2.0 \pm 0.6 (0.11 \pm 0.03)	0.17 \pm 0.12 (3.3 \pm 2.4)	2.5 \pm 2.6 (0.8 \pm 0.8)
UDP-Glc	0.4 \pm 0.1 (0.02 \pm 0.01)	5.2 \pm 0.5 (0.4 \pm 0.04)	1.4 \pm 0.3 (0.25 \pm 0.05)	2.2 \pm 0.8 (0.12 \pm 0.04)	0.22 \pm 0.02 (4.3 \pm 0.3)	3.2 \pm 0.6 (1 \pm 0.2)
UDP-GlcNAc	2.9 \pm 0.4 (0.14 \pm 0.02)	28 \pm 10 (2.5 \pm 0.9)	15 \pm 2 (2.7 \pm 0.4)	12 \pm 0.8 (0.66 \pm 0.04)	2.5 \pm 0.1 (49 \pm 2)	44 \pm 24 (14 \pm 7)
Total caps, fmol/ μ g RNA	2078 \pm 430	1131 \pm 449	566 \pm 320	1896 \pm 278	5.1 \pm 0.4	325 \pm 114

^aValues (as fmol per μ g RNA or percentage for each detected cap) represent mean \pm SD for three independent cultures for all cell lines, for tissues from three different mice, and for three technical replicates of a single culture for DENV-2 virus. nd, not detectable.

In contrast to the cap 1 structures in mammalian cells, the only canonical caps in *S. cerevisiae* were the expected cap 0 structures (m^7 GpppN), with abundances between 20 and 1524 fmol/ μ g RNA (Figure 2C and Table 1). m^7 GpppA constituted 80% of all caps (1896 fmol/ μ g), with m^7 GpppA > m^7 GpppG (16%) >> m^7 GpppU (1.5%) > m^7 GpppC (1.1%). This distribution correlates strongly with the distribution of predicted TSS frequencies in *S. cerevisiae* (Figure 3C and Supplementary Figure S6d). The four nucleotide metabolite caps were present in the *S. cerevisiae* mRNAs at abundances from 2.0 to 12.4 fmol/ μ g RNA, which is higher than in humans and mice (Figure 2A, B and Table 1). No-

tably, we found no evidence for the presence of methylated forms of A in any cap structures in yeast.

The tissue-specific variations in cap structure and quantity in mice raised the possibility that cap landscape would vary as a result of stress-specific changes in gene expression. To this idea, we quantified the cap profile in yeast exposed to well-characterized oxidative and alkylation stresses caused by hydrogen peroxide (H_2O_2) and methyl methanesulfonate (MMS), respectively. Both treatments resulted in modest changes in the levels of several caps (Figure 2C), with a significant increase in the level of UDP-GlcNAc cap (P <

0.01). However, there were no striking changes in cap levels for these two stressors.

As expected, the m⁷G-type cap structures typical of eukaryotes were not detectable in the total RNA from *E. coli* (Figure 2D and Table 1). Here we analyzed total RNA instead of mRNA because of the low prevalence of polyA tails in the *E. coli* mRNA pool, with only 2–50% of mRNAs shown to have polyA that are generally short at 14–60 nt (42). While NAD and UDP-GlcNAc were the major metabolite caps, which is consistent with the relatively high concentration of these metabolites in *E. coli* (43), the four metabolite caps in *E. coli* occurred at 10-fold lower levels than in yeast, ranging from 0.20 to 2.5 fmol/μg RNA (Figure 2D and Table 1). This suggests differing propensities of the yeast and bacterial RNA polymerases for using nucleotide metabolites to initiate transcription.

Finally, in dengue purified virion RNA genomes, the total level of detected caps amounted to 325 ± 114 fmol/μg RNA. This is consistent with nearly all copies of the ~10,700 nt RNA genome (288 fmol/μg RNA) possessing a cap. The major cap structure (70%) was found to be the cap 1 m⁷GpppAm at 226 fmol/μg RNA (Figure 2E and Table 1). Surprisingly, the cap 0 structure m⁷GpppA represented 14% of all caps. The abundance of the four metabolite caps ranged from 2.5 to 45 fmol/μg RNA, which is similar to yeast.

DISCUSSION

Here, we present CapQuant, an analytical method combining off-line HPLC enrichment with isotope-dilution LC-MS/MS analysis for analysis of the diversity and dynamics of the cap epitranscriptome. This method overcomes the shortcomings of existing cap analysis tools, which are limited to individual cap structures (20,44,45), are poorly quantitative (5,14,18), and lack of chemical specificity (5,14), to enable accurate, specific and sensitive quantification of the RNA cap landscape in any organism. It achieves high-coverage with absolute quantification—a key feature of the method—over a broad dynamic range starting at attomole levels (as little as 600 ng of RNA) and the capacity to expand to other new RNA cap structures, including the methylated guanosine caps observed in pre-tRNA (21). While isotope-labeled internal standards provide highly accurate absolute quantification, rigorous cap quantification can still be performed with external calibration curves using unlabeled standards or even with other chemically similar cap standards. The use of off-line ion-pairing HPLC (46) for cap enrichment (Figure 1B) greatly enhances quantitative sensitivity by reducing interference from the matrix and non-cap nucleotides. It further helps in new cap discoveries akin to DNA ‘adductomics’ (47) by collecting ion-pairing HPLC fractions across the elution time-course and analyzing them by MS scanning for novel MS signals. However, as the use of ion-pairing agents involves chronic contamination of HPLC and MS systems, a dedicated HPLC system and volatile ion-pairing agents for its complete removal before LC-MS/MS analysis is recommended.

Application of CapQuant to eukaryotic RNA has demonstrated that the composition of RNA caps varies between different cells and tissues, supporting the idea of a

regulated cap epitranscriptome. In addition, our data (i) quantitatively confirmed previous qualitative observations about the predominance of m⁷G-type caps, (ii) confirmed the lack of GpppN caps, (iii) facilitated the discovery of novel and noncanonical caps, such as the metabolite caps (10,12,48), (iv) revealed the potential for significant loss of m¹A and m¹Am by Dimroth-induced artifacts associated with specific RNA processing conditions, (v) showed that m¹A and m¹Am are below detectable levels in mRNA caps in human lymphoblast cells, (vi) revealed the occurrence of surprisingly high proportions of caps lacking 2'-O-methylation in mammalian mRNA and viral RNA genome and (vii) facilitated transcription start site analysis.

The lack of detectable GpppN caps could reflect the cap quality control system described in mammalian (DXO/Dom3Z protein) and yeast cells (Rail-Rat1 and Dxo1). These systems possess decapping, pyrophosphohydrolase, and 5'-to-3' exonuclease activities that appear to target caps lacking m⁷G (49,50).

With regard to m¹A, two antibody-based methods concluded that m¹A was widespread in mammalian mRNA (36,37), with subsequent studies proposing that m¹A could exist as part of a novel cap structure comprising m⁷Gpppm¹A or m⁷Gpppm¹Am (39). However, biochemical studies were not used to demonstrate the existence of these novel mRNA caps. Another study used an antibody and sequencing-based approach to detect m¹A-induced reverse transcriptase errors and suggested that m¹A was present at lower levels than previously in mRNA and long non-coding RNAs, with strong bias towards 5' termini of genes (38). Again, it remained unknown whether the enriched m¹A signals were due to the 5' terminus being a site for complex regulatory modifications or an experimental artefact. Here, we demonstrate that m¹A is unlikely to be present at appreciable levels in mRNA caps in cultured human lymphoblasts. Even after quantitatively accounting for artifactual loss of m¹A by Dimroth rearrangement to m⁶A and optimizing the CapQuant method to minimize this conversion, which amounted to ~23% in the human lymphoblasts, we did not detect m⁷GpppN or m⁷GpppNm caps containing m¹A or m¹Am in the human lymphoblasts above the limit of detection of 0.7 and 0.1 fmol, respectively. While our study does not rule out the existence of m¹A/m¹Am in mRNA caps, they are below the limits of detection of the present CapQuant method. This suggests that, if present, they are found in less than 1/16 000 and 1/100 000 mRNA transcripts, respectively, from cultured human lymphoblasts. The control studies provide a cautionary note, however, with an almost 10-fold reduction in m¹A/m¹Am levels caused by specific kits and conditions used for the yeast and mouse samples; human RNA was processed without rRNA depletion and the RNA cleanup steps, and m¹A and m¹Am losses were at most 23%. While previous sequencing-based methods reported low levels of cap m¹A in HEK293T cells (38), the existence of cap m¹A/m¹Am in different tissues or samples needs further investigation and refinement of analytical methods.

In terms of cap discovery, we detected m⁷Gpppm⁶A as a cap in mRNA from human cells and mouse liver (Figure 2A, B and Table 1). The presence of m⁷Gpppm⁶A in mouse liver but not kidney raises the possibility of a tissue-specific

role for this cap. m^7Gpppm^6A could arise by demethylation of m^7Gpppm^6Am through a yet-to-be-identified demethylase, or by N^6 -methylation of adenosine at the first transcribed nucleotide in mRNAs independent of the adenosine 2'-*O*-methylation status. While recent *in vitro* biochemical studies have shown that PCIF1, the enzyme responsible for synthesis of m^6Am in mRNA caps, can also act on m^7GpppA -capped mRNA to form m^7Gpppm^6A -capped mRNA (18,51,52). Thus, in cells, m^7GpppA caps might undergo either 2'-*O*-methylation, N^6 -methylation, or both.

CapQuant also expanded the repertoire of 5' cap structures with the discovery of three novel metabolite caps (FAD, UDP-Glc and UDP-GlcNAc) in all the RNA species analyzed (Figures 1 and 2). This expands the generality of the idea that nucleotide metabolites can serve as caps in cellular and viral RNA (2). However, metabolite caps (NAD, FAD, UDP-Glc and UDP-GlcNAc) are rare in eukaryotes, accounting for 0.3–5.1% in total of all caps detected (Figure 2 and Table 1) across eukaryotic cells and tissues. There is a strong stochastic basis for metabolite caps formation due to (i) their low abundance relative to the NpppN canonical caps in eukaryotes (>10-fold lower; 0.2–20 fmol/ μ g versus 10–600 fmol/ μ g), (ii) the similar frequencies of each cap type in all organisms, (iii) the variation in metabolite cap levels among tissues and stresses, and (iv) their proportionality to cellular metabolite pools. The role of nutrient availability and metabolite pools as determinants of metabolite cap levels is illustrated by several studies. First, it was shown by Walters *et al.* (53) that there were more NAD-capped mRNAs in *S. cerevisiae* grown in minimal medium compared to rich YEPD medium, which suggests that the levels of NAD caps are sensitive to nutrient status. Similarly, Canelas *et al.* found that NAD levels in *S. cerevisiae* are sensitive to culturing conditions and nutrient status (54). This variability in metabolite levels as a determinant of metabolite cap levels may explain the 33-fold difference in NAD caps observed here and in the studies of Grudzien-Nagolska *et al.* in *S. cerevisiae* (45), though contributions from the different analytical methods could also account for the different NAD cap levels. Finally, Grudzien-Nagolska *et al.* demonstrated that changes in cellular NAD levels in HEK293T cells correlate with changes of the levels of NAD caps (45). These studies all show a variability in metabolite cap levels based on metabolite pool levels in a way that suggests a potential signaling or regulatory function of metabolite caps. An emerging literature supports this idea. For example, the NAD cap has been shown to be present on a subset of mRNAs that are targeted for rapid decay in mammalian cells (11,55), while Kiledjian *et al.* have observed a post-transcriptional NAD capping activity, which suggests that this cap is not simply a transcriptional mistake (11).

The potential for variation in metabolite cap levels as a function of cell state is also illustrated with viral infections. For example, human cytomegalovirus (HCMV) infection upregulates UDP-GlcNAc levels in host cells (56) with similar metabolic shifts observed in other viruses (57,58). Hence it is proposed that dengue infection upregulates host cellular UDP-GlcNAc levels, especially since viral envelope (E) protein *N*-glycosylation is partly derived from UDP-GlcNAc in host cells (59,60). Higher host cell levels of

UDP-GlcNAc may lead to increased transcription initiation with this nucleotide metabolite, which would explain the relatively large proportion of UDP-GlcNAc-capped viral transcripts detected in dengue purified virions (Figure 2E and Table 1). While the biological function of these metabolite caps requires further examination, RNA Pols appear to be capable of initiating transcription with the four nucleotide metabolites studied here and that dengue virus NS5 polymerase could initiate transcription with the metabolite caps in the same manner as the host RNA Pol. However, the ability of the metabolite-capped viral genomes to sustain viral replication is unknown. In addition to the above question regarding biological function, the discovery of the three novel metabolite caps also raises several other important questions. For example, can metabolite caps be exported from the nucleus into the cytoplasm in eukaryotic cells? Are metabolite caps found in RNAs that associate with polysomes? We think that answers to these questions can be readily obtained by directly applying CapQuant to relevant systems, i.e. RNA preparations from the nucleus and cytoplasm from the same population of cells, and polysome-bound RNAs.

Consistent with published observations, we found that the cap on the dengue RNA genome isolated from purified virions contained Am but not m^6Am (Figure 2E and Table 1) as compared with human mRNA (12,61). CapQuant revealed that >30% of the viral particles generated during an infection possess caps that are counterproductive for viral replication and survival in the host: presumably untranslatable metabolite caps or the m^7GpppA cap that activates innate immunity (Figure 2E). With an estimated single copy of the RNA genome per viral particle (62) and one viral particle infecting a host cell, the varying viral cap structures detected suggest that infections will occur with viral genomes having different translational efficiency or propensity to activate the antiviral response pathways. The fate of these variously capped viral genomes in the host is largely known. Indeed, there is controversy concerning the presence of m^6Am in the caps on dengue-derived mRNAs isolated from infected cells, which presumably arise by replication of the infective genomic RNA (12,61,63). The sole published experimental work showed that only Am is found in dengue mRNA caps (63). The variable detection of m^6Am in dengue mRNA caps could be explained by contamination with the abundance of host mRNA containing m^6Am (Figure 2A and Table 1) or by N^6 -methylation of viral genomes and/or mRNA by host enzymes PCIF1 (18,51,52). Our observation that dengue genomic RNA present in purified virions lacks m^6Am in the cap implies that any N^6 -methylation of Am in caps, if required for translation, must occur in viral transcripts used for protein production. However, replicated RNA genomes destined for virion assemblies can only possess $m^7GpppAm$, m^7GpppA , and the metabolite caps, as we observed (Figure 2E and Table 1). Although some studies did not observe a global mRNA stabilizing effect of cap m^6Am (18,64,65), other studies found that cap m^6Am stabilizes subsets of mRNAs (24,51). Interestingly, N^6 -methylation of A within the viral mRNA has been found to negatively regulate viral infec-

tion by reducing viral particle formation (66), while we have previously demonstrated that Am is present throughout the RNA genome of purified dengue virions (23). Clearly, there is significant work to be done to clarify the capping mechanisms involved in the various steps of viral infection.

CapQuant also showed that 14% of dengue genomes possess m⁷GpppA cap, and that 12% of human and 3% of mouse liver mRNAs possess m⁷Gpppm⁶A caps (Figure 2 and Table 1). This observation of the latter stands in contrast to the inability to detect it in a crude, chemically-nonspecific TLC method (5) or in insensitive LC-MS studies lacking standards (18). Although it is possible that m⁷Gpppm⁶A cap was indeed absent in those RNA preparations, the failure to detect this cap could also be due to lack of chemical specificity and insufficient sensitivity of the two-dimensional TLC method (5) or, in the LC-MS method, due to a lack of sensitivity and to the selected monitoring of m⁷G-capped dimers (m⁷GpppN₁Gp) to pentamers (m⁷GpppN₁N₂N₃N₄Gp) containing 0–3 methyl groups, which include only a portion of all possible m⁷G-capped sequences with A or methylated A as the first transcribed nucleotide (18). The detection of m⁷Gpppm⁶A caps in the present studies is rigorously and unambiguously established based on the identical chromatographic behavior and mass spectrometrically-defined structural identity with a synthetic standard.

The presence of m⁷Gpppm⁶A caps in human and mouse liver mRNAs is unlikely due to inefficient cellular 2'-O-methyltransferase activities or insufficient cellular innate immunity targeting cap 0 structures (67) since none of the other cap 0 structures were detectable in these RNAs, even in human CCRF-SB mRNA where the levels of m⁷GpppCm, m⁷GpppGm and m⁷GpppAm were up to 2-fold higher than m⁷Gpppm⁶Am (Figure 2 and Table 1). Thus, these data suggest that, at least in some cell types, 2'-O-methylation is not present on all mRNAs, suggesting that there may be specific cellular contexts in which 2'-O-methylation is not needed to suppress the innate host antiviral response (3), or that 2'-O-methylation is rate-limiting and we are detecting an elevated level of intermediate, precursor cap structures that are not present long enough to activate the host innate response. It is well established that RIG-I and MDA5 are sensors of non-self RNA in mammalian cells, and the IFIT complex is a dual sensor-effector of a cellular innate defense system (67) for caps without 2'-O-methylation. IFIT complex recognizes m⁷GpppA cap structures to inhibit translation of the viral genome during viral infection (3) while RIG-I binds to dsRNA with 5'-ppp and cap 0 (68). 2'-O-Methylated caps (5'-pppNm and m⁷GpppNm) significantly reduces RIG-I binding affinity to target RNA and the innate defense system activation (68). This raises an important question: Does the proportion of m⁷GpppA caps present during a dengue infection correlate with virulence? It is reasonable to hypothesize that the more virulent dengue strains have evolved to minimize the proportion of m⁷GpppA caps that activate the innate antiviral response in host cells, a hypothesis readily tested by application of CapQuant to clinical dengue isolates replicated in culture.

Interestingly, the level of m⁷Gpppm⁶A cap in mRNA differed significantly among human CCRF-SB, mouse liver

and mouse kidney (Figure 2A and B). To explore if these differences are linked to expression of relevant cap modification enzymes, we assessed the relative mRNA levels (RT-qPCR) of a variety of RNA cap modification enzymes, including PCIF1, FTO, DCP2, CMTR1 and ALKBH5 in the total RNA from CCRF-SB cells and mouse liver and kidney tissues. We observed no significant difference in transcript levels for the enzymes among the cells and tissues (Supplementary Figure S12). This suggests that the different levels of m⁷Gpppm⁶A cap are likely due to regulation of enzyme activity at the level of translation or protein secondary modification. By whatever mechanism, our observations of the cap landscape in mouse tissues agree well with the studies of Suzuki and coworkers (18). They observed that m⁷Gpppm⁶Am represented 92% of cap structures in human HEK293 cells, with undetectable levels of m⁷Gpppm⁶AG leading them to conclude that m⁷GpppAm formation precedes m⁷Gpppm⁶Am. Loss of PCIF1 led to mainly m⁷GpppAm in the HEK293 cells. We observed 85% m⁷Gpppm⁶Am in mouse liver (9% m⁷GpppAm, 6% m⁷Gpppm⁶A) and 93% m⁷Gpppm⁶Am in mouse kidney (7% m⁷GpppAm, no detectable m⁷Gpppm⁶A). However, we observed nearly equal proportions of m⁷Gpppm⁶A, m⁷Gpppm⁶Am, and m⁷GpppAm in human CCRF-SB lymphoblast cells, which contrasts with the predominance (92%) of m⁷Gpppm⁶Am in HEK293 cells. This might indicate differential activity of PCIF1 in the two immortalized cell lines.

CapQuant analysis also provided strong corroboration for TSS studies, which are challenging due to the lack of long and conserved consensus sequences for TSSs. m⁷G caps with a purine as the first transcribed nucleotide represented the major caps found in mRNAs from human CCRF-SB (70%), mouse liver (82%) and kidney (74%) tissues, and *S. cerevisiae* W1588-4C (97%), with the relative abundance of different m⁷GpppNm's or m⁷GpppN's varying across the organisms and tissues (Figure 2A, C and Table 1). This preference for purines at the penultimate position in m⁷GpppN caps is rationalized by the strong preference for pyrimidine-purine dinucleotides at -1 and +1 positions of TSSs in the coding strand of eukaryotes, bacteria and some viruses, which is argued to facilitate the loading of ATP or GTP during transcription initiation (69–71). A comparison of the distribution of the second nucleotide in m⁷GpppN/m⁷GpppNm caps revealed by CapQuant to the distribution of TSSs (+1 position) predicted using the cap analysis gene expression (CAGE) method (29,72) was conducted for cross-validation. The CAGE method is advantageous over other TSS analysis methods in that it only captures capped transcripts and thus avoids false TSSs from degraded transcripts that do not contain caps. We observed a strong correlation between the cap second nucleotide distribution and the TSS distribution for *S. cerevisiae*, mice and humans (Figure 3A-C and Supplementary Figure S6b-d).

CapQuant is not without limitations and there are unanswered questions that arise from the results. For example, the level of all caps per μg of mRNA in the mouse tissues was about 2- to 4-fold lower than in human cells and yeast, and mouse liver and kidney differed by 2-fold (Table 1). There are several possible explanations for this variance. First, contamination of the poly(A)-purified mRNA with

non-capped or decapped RNA would dilute the analyzed caps. While it is possible that RNA contamination could contribute to the observed differences, gross contamination with rRNA or other non-coding RNAs was not apparent in Bioanalyzer profiles of the cell and tissue mRNA preparations (Supplementary Figure S4; compare rRNA-depleted yeast and mouse samples to human samples; also compare proportional signal intensities to Bioanalyzer electropherograms in total RNA samples in Supplementary Figure S5). More importantly, contamination with non-capped or uncapped RNA would cause the levels for all caps to decrease to the same extent across samples. The data in Table 1 show that this is not the case for the non-canonical caps, which are 3.8- to 13-fold higher in the mouse tissues compared to human cells in spite of the 1.8- to 3.7-fold higher level of total caps in human mRNA samples. This suggests that simple RNA contamination cannot fully explain the different total cap levels among cells and tissues.

A second mechanism that could account for variance in cap levels involves differential activity of capping and decapping enzymes as well as overall RNA decay in the cells and tissues. This is illustrated for capping enzymes by the differences in m⁷Gpppm⁶A levels discussed earlier. Decapping activity is involved in two mechanisms regulating mRNA stability: 3'-5' and 5'-3' RNA decay. The RNA in the human cells, mouse tissues, and yeast cells was purified by poly(T) affinity chromatography, so differences in the 5'-3' RNA decay pathways, which remove the poly(A) tail first (73,74), cannot explain the variance. However, there is a growing number of RNA decapping enzymes in eukaryotic cells, including Dcp2 and 7 Nudt enzymes in human cells, with expression of the decapping enzymes varying significantly among tissues (75). It is thus quite possible that the variation in total cap levels among human cells, mouse tissues, and yeast reflects a complicated balance of the different levels of transcriptional activity, capping and decapping enzyme activity, and other contributors to RNA decay.

It should also be noted that in human, *S. cerevisiae*, and *E. coli* cells, the levels of NAD cap revealed in the present study (Table 1) are up to 55-fold lower than those levels of the same cap determined or estimated in other studies (20,45). In addition to the variable accuracy of the different analytical methods, lower levels of NAD detection in the present studies could be due, at least in part, to differences in the cell culture conditions (45,53,54) and cell strains used in the different studies, as discussed earlier. In the case of *E. coli*, we analyzed caps in stationary-phase cells whereas Chen *et al.* analyzed caps in log-phase *E. coli* (20), which could contribute to the lower NAD cap level observed in our study. In addition, the non-significant changes in the abundance of NAD in the control experiments by Chen *et al.* (20) when spiking large amounts of NAD into the cell lysate prior to RNA isolation cannot rule out the possibility that the NAD they detected in the samples represented contaminating non-covalently bound NAD. CapQuant employs isotopically-labeled internal standards for cap quantification, which enhances the accuracy of the method.

In summary, CapQuant is a widely applicable method for precise and accurate quantitation of the RNA cap landscape in cells and tissues. The method is readily applied to study the function of specific caps, of caps on different

types of non-coding RNAs, of the dynamics and regulation of RNA capping and decapping, and of the roles that capping proteins, such as eIF4E and CBC, in the control of gene expression (76). When combined with transcript-specific purification technology (77), CapQuant would enable quantification of cap structures in specific transcripts and thus studies of transcript-specific capping and decapping, and gene-specific regulation.

SUPPLEMENTARY DATA

Supplementary Data are available at NAR Online.

ACKNOWLEDGEMENTS

We thank Profs. Graham Walker and Jianzhu Chen from the Massachusetts Institute of Technology for generously sharing *S. cerevisiae* W1588-4C and human CCRF-SB cells, respectively.

FUNDING

National Institutes of Health [ES022858 to P.C.D. and CA186702 to S.R.J.]; Singapore-MIT Alliance for Research and Technology with a grant from the National Research Foundation of Singapore; Inner Mongolia University with a grant from its 'Steed Plan' High-Level Talents Program (awarded to J.W.); Nanyang Presidential Graduate Scholarship (to B.L.A.C.). Funding for open access charge: National Research Foundation Singapore.

Conflict of interest statement. S.R.J. is scientific founder, advisor to, and owns equity in Gotham Therapeutics.

REFERENCES

- Helm, M. and Alfonzo, J.D. (2014) Posttranscriptional RNA Modifications: playing metabolic games in a cell's chemical Legoland. *Chem. Biol.*, **21**, 174–185.
- Ramanathan, A., Robb, G.B. and Chan, S.H. (2016) mRNA capping: biological functions and applications. *Nucleic Acids Res.*, **44**, 7511–7526.
- Hyde, J.L. and Diamond, M.S. (2015) Innate immune restriction and antagonism of viral RNA lacking 2-O methylation. *Virology*, **479–480**, 66–74.
- Kastern, W.H. and Berry, S.J. (1976) Non-methylated guanosine as 5' terminus of capped messenger-rna from insect oocytes. *Biochem. Biophys. Res. Commun.*, **71**, 37–44.
- Wei, C., Gershowitz, A. and Moss, B. (1975) N⁶, O^{2'}-dimethyladenosine a novel methylated ribonucleoside next to the 5' terminal of animal cell and virus mRNAs. *Nature*, **257**, 251–253.
- Hsu, C.C. and Dubin, D.T. (1976) Di- and trimethylated congeners of 7-methylguanine in Sindbis virus mRNA. *Nature*, **264**, 190–191.
- Byszewska, M., Smietanski, M., Purta, E. and Bujnicki, J.M. (2014) RNA methyltransferases involved in 5' cap biosynthesis. *RNA Biol.*, **11**, 1597–1607.
- Bird, J.G., Zhang, Y., Tian, Y., Panova, N., Barvik, I., Greene, L., Liu, M., Buckley, B., Krasny, L., Lee, J.K. *et al.* (2016) The mechanism of RNA 5' capping with NAD⁺, NADH and desphospho-CoA. *Nature*, **535**, 444–447.
- Julius, C. and Yuzenkova, Y. (2017) Bacterial RNA polymerase caps RNA with various cofactors and cell wall precursors. *Nucleic Acids Res.*, **45**, 8282–8290.
- Jaschke, A., Hofer, K., Nubel, G. and Frindert, J. (2016) Cap-like structures in bacterial RNA and epitranscriptomic modification. *Curr. Opin. Microbiol.*, **30**, 44–49.

11. Kiledjian, M. (2018) Eukaryotic RNA 5'-End NAD⁺ Capping and DeNADding. *Trends Cell Biol.*, **28**, 454–464.
12. Furuichi, Y. (2015) Discovery of m⁷G-cap in eukaryotic mRNAs. *Proc. Jpn. Acad. Ser. B*, **91**, 394–409.
13. Shatkin, A.J. (1976) Capping of eucaryotic mRNAs. *Cell*, **9**, 645–653.
14. Wei, C.M., Gershowitz, A. and Moss, B. (1976) 5'-Terminal and internal methylated nucleotide sequences in HeLa cell mRNA. *Biochemistry*, **15**, 397–401.
15. Cleaver, J.E. and Burki, H.J. (1974) Letter: Biological damage from intranuclear carbon-14 decays: DNA single-strand breaks and repair in mammalian cells. *Int. J. Radiat. Biol. Relat. Stud. Phys. Chem. Med.*, **26**, 399–403.
16. Minor, R.R. (1982) Cytotoxic effects of low levels of ³H-, ¹⁴C-, and ³⁵S-labeled amino acids. *J. Biol. Chem.*, **257**, 10400–10413.
17. Abdelhamid, R.F., Plessy, C., Yamauchi, Y., Taoka, M., de Hoon, M., Gingeras, T.R., Isobe, T. and Carninci, P. (2014) Multiplicity of 5' cap structures present on short RNAs. *PLoS One*, **9**, e102895.
18. Akichika, S., Hirano, S., Shichino, Y., Suzuki, T., Nishimasu, H., Ishitani, R., Sugita, A., Hirose, Y., Iwasaki, S., Nureki, O. *et al.* (2019) Cap-specific terminal N⁶-methylation of RNA by an RNA polymerase II-associated methyltransferase. *Science*, **363**, eaav0080.
19. Beverly, M., Dell, A., Parmar, P. and Houghton, L. (2016) Label-free analysis of mRNA capping efficiency using RNase H probes and LC-MS. *Anal. Bioanal. Chem.*, **408**, 5021–5030.
20. Chen, Y.G., Kowtoniuk, W.E., Agarwal, I., Shen, Y. and Liu, D.R. (2009) LC/MS analysis of cellular RNA reveals NAD-linked RNA. *Nat. Chem. Biol.*, **5**, 879–881.
21. Ohira, T. and Suzuki, T. (2016) Precursors of tRNAs are stabilized by methylguanosine cap structures. *Nat. Chem. Biol.*, **12**, 648–655.
22. Peyrane, F., Selisko, B., Decroly, E., Vasseur, J.J., Benarroch, D., Canard, B. and Alvarez, K. (2007) High-yield production of short GpppA- and (7Me)GpppA-capped RNAs and HPLC-monitoring of methyltransfer reactions at the guanine-N7 and adenosine-2' O positions. *Nucleic Acids Res.*, **35**, e26.
23. Dong, H., Chang, D.C., Hua, M.H., Lim, S.P., Chionh, Y.H., Hia, F., Lee, Y.H., Kukkaro, P., Lok, S.M., Dedon, P.C. *et al.* (2012) 2'-O methylation of internal adenosine by flavivirus NS5 methyltransferase. *PLoS Pathog.*, **8**, e1002642.
24. Mauer, J., Luo, X., Blanjoie, A., Jiao, X., Grozhik, A.V., Patil, D.P., Linder, B., Pickering, B.F., Vasseur, J.J., Chen, Q. *et al.* (2017) Reversible methylation of m(6)Am in the 5' cap controls mRNA stability. *Nature*, **541**, 371–375.
25. Wang, J., Dong, H., Chionh, Y.H., McBee, M.E., Sirirungruang, S., Cunningham, R.P., Shi, P.Y. and Dedon, P.C. (2016) The role of sequence context, nucleotide pool balance and stress in 2'-deoxynucleotide misincorporation in viral, bacterial and mammalian RNA. *Nucleic Acids Res.*, **44**, 8962–8975.
26. Kodzius, R., Kojima, M., Nishiyori, H., Nakamura, M., Fukuda, S., Tagami, M., Sasaki, D., Imamura, K., Kai, C., Harbers, M. *et al.* (2006) CAGE: cap analysis of gene expression. *Nat. Methods*, **3**, 211–222.
27. Kanamori-Katayama, M., Itoh, M., Kawaji, H., Lassmann, T., Katayama, S., Kojima, M., Bertin, N., Kaiho, A., Ninomiya, N., Daub, C.O. *et al.* (2011) Unamplified cap analysis of gene expression on a single-molecule sequencer. *Genome Res.*, **21**, 1150–1159.
28. Carninci, P., Kvam, C., Kitamura, A., Ohsumi, T., Okazaki, Y., Itoh, M., Kamiya, M., Shibata, K., Sasaki, N., Izawa, M. *et al.* (1996) High-efficiency full-length cDNA cloning by biotinylated CAP trapper. *Genomics*, **37**, 327–336.
29. Lu, Z. and Lin, Z. (2019) Pervasive and dynamic transcription initiation in *Saccharomyces cerevisiae*. *Genome Res.*, **29**, 1198–1210.
30. Lizio, M., Harshbarger, J., Shimoji, H., Severin, J., Kasukawa, T., Sahin, S., Abugessaisa, I., Fukuda, S., Hori, F., Ishikawa-Kato, S. *et al.* (2015) Gateways to the FANTOM5 promoter level mammalian expression atlas. *Genome Biol.*, **16**, 22.
31. Lizio, M., Harshbarger, J., Abugessaisa, I., Noguchi, S., Kondo, A., Severin, J., Mungall, C., Arenillas, D., Mathelier, A., Medvedeva, Y.A. *et al.* (2017) Update of the FANTOM web resource: high resolution transcriptome of diverse cell types in mammals. *Nucleic Acids Res.*, **45**, D737–D743.
32. Afgan, E., Baker, D., Batut, B., van den Beek, M., Bouvier, D., Cech, M., Chilton, J., Clements, D., Coraor, N., Gruning, B.A. *et al.* (2018) The Galaxy platform for accessible, reproducible and collaborative biomedical analyses: 2018 update. *Nucleic Acids Res.*, **46**, W537–W544.
33. Quinlan, A.R. and Hall, I.M. (2010) BEDTools: a flexible suite of utilities for comparing genomic features. *Bioinformatics*, **26**, 841–842.
34. Vandesompele, J., De Preter, K., Pattyn, F., Poppe, B., Van Roy, N., De Paep, A. and Speleman, F. (2002) Accurate normalization of real-time quantitative RT-PCR data by geometric averaging of multiple internal control genes. *Genome Biol.*, **3**, RESEARCH0034.
35. Abraham, G., Rhodes, D.P. and Banerjee, A.K. (1975) The 5' terminal structure of the methylated mRNA synthesized in vitro by vesicular stomatitis virus. *Cell*, **5**, 51–58.
36. Dominissini, D., Nachtergale, S., Moshitch-Moshkovitz, S., Peer, E., Kol, N., Ben-Haim, M.S., Dai, Q., Di Segni, A., Salmon-Divon, M., Clark, W.C. *et al.* (2016) The dynamic N(1)-methyladenosine methylome in eukaryotic messenger RNA. *Nature*, **530**, 441–446.
37. Li, X., Xiong, X., Wang, K., Wang, L., Shu, X., Ma, S. and Yi, C. (2016) Transcriptome-wide mapping reveals reversible and dynamic N(1)-methyladenosine methylome. *Nat. Chem. Biol.*, **12**, 311–316.
38. Safra, M., Sas-Chen, A., Nir, R., Winkler, R., Nachshon, A., Bar-Yaacov, D., Erlacher, M., Rossmannith, W., Stern-Ginossar, N. and Schwartz, S. (2017) The m1A landscape on cytosolic and mitochondrial mRNA at single-base resolution. *Nature*, **551**, 251–255.
39. Li, X., Xiong, X., Zhang, M., Wang, K., Chen, Y., Zhou, J., Mao, Y., Lv, J., Yi, D., Chen, X.W. *et al.* (2017) Base-resolution mapping reveals distinct m(1)A methylome in nuclear- and mitochondrial-encoded transcripts. *Mol. Cell*, **68**, 993–1005.
40. Namboori, S.C. and Graham, D.E. (2008) Enzymatic analysis of uridine diphosphate N-acetyl-D-glucosamine. *Anal. Biochem.*, **381**, 94–100.
41. Yang, H., Yang, T., Baur, J.A., Perez, E., Matsui, T., Carmona, J.J., Lammung, D.W., Souza-Pinto, N.C., Bohr, V.A., Rosenzweig, A. *et al.* (2007) Nutrient-sensitive mitochondrial NAD⁺ levels dictate cell survival. *Cell*, **130**, 1095–1107.
42. Sarkar, N. (1997) Polyadenylation of mRNA in prokaryotes. *Annu. Rev. Biochem.*, **66**, 173–197.
43. Bennett, B.D., Kimball, E.H., Gao, M., Osterhout, R., Van Dien, S.J. and Rabinowitz, J.D. (2009) Absolute metabolite concentrations and implied enzyme active site occupancy in *Escherichia coli*. *Nat. Chem. Biol.*, **5**, 593–599.
44. Cahova, H., Winz, M.-L., Höfer, K., Nübel, G. and Jäschke, A. (2015) NAD captureSeq indicates NAD as a bacterial cap for a subset of regulatory RNAs. *Nature*, **519**, 374–377.
45. Grudzien-Nogalska, E., Bird, J.G., Nickels, B.E. and Kiledjian, M. (2018) “NAD-capQ” detection and quantitation of NAD caps. *RNA*, **24**, 1418–1425.
46. Liu, S. and Wang, Y. (2015) Mass spectrometry for the assessment of the occurrence and biological consequences of DNA adducts. *Chem. Soc. Rev.*, **44**, 7829–7854.
47. Balbo, S., Turesky, R.J. and Villalta, P.W. (2014) DNA adductomics. *Chem. Res. Toxicol.*, **27**, 356–366.
48. Ghosh, A. and Lima, C.D. (2010) Enzymology of RNA cap synthesis. *Wiley Interdiscip. Rev. RNA*, **1**, 152–172.
49. Jiao, X., Xiang, S., Oh, C., Martin, C.E., Tong, L. and Kiledjian, M. (2010) Identification of a quality-control mechanism for mRNA 5'-end capping. *Nature*, **467**, 608–611.
50. Jiao, X., Chang, J.H., Kilic, T., Tong, L. and Kiledjian, M. (2013) A mammalian pre-mRNA 5' end capping quality control mechanism and an unexpected link of capping to pre-mRNA processing. *Mol. Cell*, **50**, 104–115.
51. Boulias, K., Toczyłowska-Socha, D., Hawley, B., Liberman-Isakov, N., Takashima, K., Zaccara, S., Guez, T., Vasseur, J.-J., Debart, F., Aravind, L. *et al.* (2019) Identification of the m⁶Am methyltransferase PCIF1 reveals the location and functions of m⁶Am in the transcriptome. *Mol. Cell*, **75**, 631–643.
52. Sun, H., Zhang, M., Li, K., Bai, D. and Yi, C. (2019) Cap-specific, terminal N⁶-methylation by a mammalian m⁶Am methyltransferase. *Cell Res.*, **29**, 80–82.
53. Walters, R.W., Matheny, T., Mizoue, L.S., Rao, B.S., Muhlrad, D. and Parker, R. (2017) Identification of NAD⁺ capped mRNAs in *Saccharomyces cerevisiae*. *Proc. Natl. Acad. Sci. U.S.A.*, **114**, 480–485.
54. Canelas, A.B., van Gulik, W.M. and Heijnen, J.J. (2008) Determination of the cytosolic free NAD/NADH ratio in *Saccharomyces cerevisiae* under steady-state and highly dynamic conditions. *Biotechnol. Bioeng.*, **100**, 734–743.

55. Jiao, X., Doamekpor, S.K., Bird, J.G., Nickels, B.E., Tong, L., Hart, R.P. and Kiledjian, M. (2017) 5' End nicotinamide adenine dinucleotide cap in human cells promotes RNA decay through DXO-mediated deNADding. *Cell*, **168**, 1015–1027.
56. DeVito, S.R., Ortiz-Riano, E., Martinez-Sobrido, L. and Munger, J. (2014) Cytomegalovirus-mediated activation of pyrimidine biosynthesis drives UDP-sugar synthesis to support viral protein glycosylation. *Proc. Natl. Acad. Sci. U.S.A.*, **111**, 18019–18024.
57. Enav, H., Mandel-Gutfreund, Y. and Beja, O. (2014) Comparative metagenomic analyses reveal viral-induced shifts of host metabolism towards nucleotide biosynthesis. *Microbiome*, **2**, 9.
58. Li, H., Zhu, W., Zhang, L., Lei, H., Wu, X., Guo, L., Chen, X., Wang, Y. and Tang, H. (2015) The metabolic responses to hepatitis B virus infection shed new light on pathogenesis and targets for treatment. *Sci. Rep.*, **5**, 8421.
59. Banerjee, S., Vishwanath, P., Cui, J., Kelleher, D.J., Gilmore, R., Robbins, P.W. and Samuelson, J. (2007) The evolution of N-glycan-dependent endoplasmic reticulum quality control factors for glycoprotein folding and degradation. *Proc. Natl. Acad. Sci. U.S.A.*, **104**, 11676–11681.
60. Yap, S.S.L., Nguyen-Khuong, T., Rudd, P.M. and Alonso, S. (2017) Dengue virus glycosylation: What do we know? *Front. Microbiol.*, **8**, 1415.
61. Banerjee, A.K. (1980) 5'-terminal cap structure in eucaryotic messenger ribonucleic acids. *Microbiol. Rev.*, **44**, 175–205.
62. Kuhn, R.J., Zhang, W., Rossmann, M.G., Pletnev, S.V., Corver, J., Lenches, E., Jones, C.T., Mukhopadhyay, S., Chipman, P.R., Strauss, E.G. et al. (2002) Structure of dengue virus: implications for flavivirus organization, maturation, and fusion. *Cell*, **108**, 717–725.
63. Cleaves, G.R. and Dubin, D.T. (1979) Methylation status of intracellular dengue type 2 40 S RNA. *Virology*, **96**, 159–165.
64. Sendinc, E., Valle-Garcia, D., Dhall, A., Chen, H., Henriques, T., Navarrete-Perea, J., Sheng, W., Gygi, S.P., Adelman, K. and Shi, Y. (2018) PCIF1 catalyzes m⁶Am mRNA methylation to regulate gene expression. *Mol. Cell*, **75**, 620–630.
65. Wei, J., Liu, F., Lu, Z., Fei, Q., Ai, Y., He, P.C., Shi, H., Cui, X., Su, R., Klungland, A. et al. (2018) Differential m⁶A, m⁶Am, and m¹A demethylation mediated by FTO in the cell nucleus and cytoplasm. *Mol. Cell*, **71**, 973–985.
66. Gokhale, N.S., McIntyre, A.B.R., McFadden, M.J., Roder, A.E., Kennedy, E.M., Gandara, J.A., Hopcraft, S.E., Quicke, K.M., Vazquez, C., Willer, J. et al. (2016) N⁶-Methyladenosine in Flaviviridae viral RNA genomes regulates infection. *Cell Host Microbe*, **20**, 654–665.
67. Mears, H.V. and Sweeney, T.R. (2018) Better together: the role of IFIT protein-protein interactions in the antiviral response. *J. Gen. Virol.*, **99**, 1463–1477.
68. Chow, K.T., Gale, M. Jr and Loo, Y.M. (2018) RIG-I and other RNA sensors in antiviral immunity. *Annu. Rev. Immunol.*, **36**, 667–694.
69. Basu, R.S., Warner, B.A., Molodtsov, V., Pupov, D., Esyunina, D., Fernandez-Tornero, C., Kulbachinskiy, A. and Murakami, K.S. (2014) Structural basis of transcription initiation by bacterial RNA polymerase holoenzyme. *J. Biol. Chem.*, **289**, 24549–24559.
70. Gleghorn, M.L., Davydova, E.K., Basu, R., Rothman-Denes, L.B. and Murakami, K.S. (2011) X-ray crystal structures elucidate the nucleotidyl transfer reaction of transcript initiation using two nucleotides. *Proc. Natl. Acad. Sci. U.S.A.*, **108**, 3566–3571.
71. Zhang, Y., Degen, D., Ho, M.X., Sineva, E., Ebright, K.Y., Ebright, Y.W., Mekler, V., Vahedian-Movahed, H., Feng, Y., Yin, R. et al. (2014) GE23077 binds to the RNA polymerase 'i' and 'i+1' sites and prevents the binding of initiating nucleotides. *Elife*, **3**, e02450.
72. Noguchi, S., Arakawa, T., Fukuda, S., Furuno, M., Hasegawa, A., Hori, F., Ishikawa-Kato, S., Kaida, K., Kaiho, A., Kanamori-Katayama, M. et al. (2017) FANTOM5 CAGE profiles of human and mouse samples. *Sci. Data*, **4**, 170112.
73. Labno, A., Tomecki, R. and Dziembowski, A. (2016) Cytoplasmic RNA decay pathways - enzymes and mechanisms. *Biochim. Biophys. Acta*, **1863**, 3125–3147.
74. Mugridge, J.S., Collier, J. and Gross, J.D. (2018) Structural and molecular mechanisms for the control of eukaryotic 5'-3' mRNA decay. *Nat. Struct. Mol. Biol.*, **25**, 1077–1085.
75. Song, M.G., Li, Y. and Kiledjian, M. (2010) Multiple mRNA decapping enzymes in mammalian cells. *Mol. Cell*, **40**, 423–432.
76. Topisirovic, I., Svitkin, Y.V., Sonenberg, N. and Shatkin, A.J. (2011) Cap and cap-binding proteins in the control of gene expression. *Wiley Interdiscip. Rev. RNA*, **2**, 277–298.
77. Adams, N.M., Bordelon, H., Wang, K.K., Albert, L.E., Wright, D.W. and Haselton, F.R. (2015) Comparison of three magnetic bead surface functionalities for RNA extraction and detection. *ACS Appl. Mater. Interfaces*, **7**, 6062–6069.